Effects of the preferential segregation of droplets on evaporation and turbulent mixing

JULIEN REVEILLON
AND FRANCOIS-XAVIER DEMOULIN

University of Rouen, CORIA UMR-CNRS, 6614, Avenue de l'Université,
76801 Saint Etienne du Rouvray, France
reveillon@coria.fr

Droplet segregation in isotropic homogeneous turbulence is analysed using a spectral direct numerical simulation solver to describe the evolution of the turbulent carrier phase, whose characteristic properties remain statistically stationary due to a semi-deterministic forcing scheme. Lagrangian dilute spray modelling is employed to describe the discrete-phase evolution. The liquid density is distributed on an Eulerian mesh to analyse the evolution of the spray and its spatial distribution. This gives results in accordance with classical methods for droplet segregation. It also allows a deeper analysis of the spray evolution. In particular, droplet segregation and vapour mass fraction may be analysed jointly. First, droplet segregation phenomena are studied through the analysis of the formation and the geometry of the droplet clusters. Then, the effects of segregation on spray evaporation are investigated from both the dispersed and carrier phase points of view. At equilibrium, droplet dynamics leads to different segregation levels that are associated with characteristic Stokes numbers. It appears that the evaporation process evolves in three different stages in time: single-droplet mode in the early stage, cluster mode in the intermediate stage and a gaseous mode in the late stage. Segregation levels strongly affect the evolution of the mean vapour mixture fraction during the second stage, while the corresponding standard deviation is affected for longer, up to the third stage in our simulations. However, from the evolution of the integral scale and the shape of the energy spectrum, it appears that turbulent mixing eliminates the segregation effects, apart from the first evaporation stage when the droplet segregation determines the vapour distribution.

1. Introduction

In industrial systems involving energy transport or transformation, a combustion chamber is generally fuelled by a spray of evaporating liquid droplets. Depending on the chamber's geometry, the spray injection conditions and the mixing phenomena, various combustion regimes and flame structures may be observed, from premixed flames to diffusion flames. However, partially premixed combustion is generally observed because of the triple interactions between spray, turbulence and combustion. The modelling of such chambers, involving the combustion of a two-phase flow or of a gaseous mixture released by the evaporation of a spray, is of primary importance in improving the output of a device and predicting pollutant formation while still maintaining a reasonable development cost.

One of the main input parameters of any non-premixed turbulent combustion model is the mixture fraction variable (denoted Z in this paper), which characterizes

locally the mixing between the evaporated fuel and the gaseous oxidizer. In Reynolds-averaged (RANS) modelling and according to the selected combustion model, the mean mixture fraction, its variance and its dissipation rate allow the generation of probability density functions (PDFs), (Borghi 1988) or localization in flamelet libraries (Peters 1986). These parameters are also the basis of conditional moment closure methods (Klimenko & Bilger 1999). Note that within the framework of large-eddy simulations (LES), analogous data have to be determined at a subgrid level.

Much work has been dedicated to predicting the mixture fraction evolution in purely gaseous flows where Z is an inert scalar: the evolution of its averaged value $\overline{Z}$ is classically established through an advection/diffusion equation, although determining its variance $\overline{Z'^2}$ and dissipation χ_Z is less straightforward; see for instance Newman, Launder & Lumley (1982), Mantel & Borghi (1994) and references therein. The difficulties are now well understood and many closures exist. However, when two-phase flows are considered, the mixture fraction is no longer an inert scalar: the appearance, in the gas phase, of mass source terms due to the evaporation of the liquid phase strongly modifies the mixture fraction field. According to the local droplet density, Z fluctuations appear during the turbulent mixing and the local rise of mixture fraction gradients affects the dissipation rate. The formalism of these new source terms and their effects on the gas phase have been described in Reveillon, Bray & Vervisch (1998), Reveillon & Vervisch (2000), Demoulin & Borghi (2002) and Colin & Benkenida (2003) where new closures have been suggested. These models evaluate the new source terms appearing in the transport equations for mixture fraction mean and variance, and take into account the evaporation effects on the dissipation level and the mixing delay.

However, while interesting data about the effects of these mass source terms have been gathered, there is a lack of information concerning their spatial distribution. Indeed, prior to the determination of the gas-phase turbulent mixing, dispersion of evaporating droplets is a major phenomenon that directly affects the evolution of the mixture fraction. Although the dispersion of particles embedded in turbulent flows is one of the major research fields of two-phase flow, no direct link has been made between the droplet turbulent dispersion, the mass source term distribution and the mixture fraction evolution in a generic configuration.

The objective of this paper is to describe the simultaneous effects of turbulence on spray dispersion and mixture fraction evolution. A direct numerical simulation (DNS) solver is coupled with a Lagrangian model to describe the evolution of an evaporating spray in a turbulent flow. Thus, the main characteristics of the mixture fraction field (fluctuation intensity levels and characteristic length scales) are estimated directly with respect to the local properties of the turbulence (r.m.s., length scales) and the spray parameters (Stokes number, liquid equivalence ratio).

As sketched in figure 1, multiple interactions between the turbulent flow, the spray dispersion and the vapour micro-mixing may be defined. To reduce the number of varying parameters, a simplified configuration very close to the one used by Eswaran & Pope (1988), for their reference study of the turbulent mixing of purely gaseous flow, has been extended to two-phase flow simulations. Thus, forced isotropic homogeneous turbulence, with statistically stationary properties, is used as the carrier phase. A recently developed forcing scheme (Guichard, Reveillon & Hauguel 2004) allowing stable mean properties of the turbulence to be obtained (energy, dissipation, integral length scale) has been introduced in a spectral formulation describing the evolution of the gas phase.
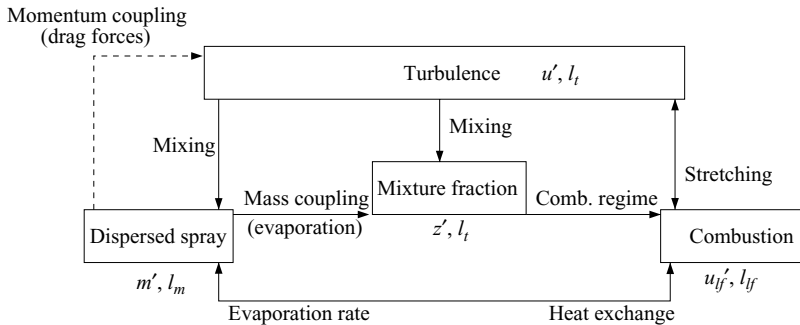
FIGURE 1. Sketch of direct and indirect mixing due to turbulence. General objective: analysis of spray combustion.

Over the last decade, DNS has been widely used in a large range of applications. It was first introduced for inert flow simulations (Orszag & Patterson 1972; Rogallo 1981; Lee, Lele & Moin 1991) and has been extended to reactive flows in order to study non-premixed, partially premixed and premixed turbulent combustion of purely gaseous fluids (Givi 1989; Poinsot, Candel & Trouvé 1996; Vervisch & Poinsot 1998; Poinsot & Veynante 2001; Pantano, Sarkar & Williams 2003). DNS was first extended to two-phase flows in the pioneering work of Riley & Patterson (1974). Most of the early numerical studies were on solid particle dispersion (see for instance: Samimy & Lele 1991; Squires & Eaton 1991; Elgobashi & Truesdell 1992; Wang & Maxey 1993; Ling *et al.* 1998). Mashayek *et al.* (1997) conducted one of the first DNS of evaporating droplets in turbulent flows. They neglected the effect of the spray on the carrier phase (one-way coupling) and they assumed an incompressible flow. Since then, DNS of two-phase flows have been extended to incorporate two-way coupling effects and to deal with spray evaporation and combustion phenomena (Mashayek 1998; Miller & Bellan 1999, 2000; Reveillon & Vervisch 2005).

In this work, various physical processes are analysed from three-dimensional simulations following a two-stage procedure. First, the turbulent dispersion of an initially randomly dispersed spray is considered with non-evaporating particles. The formation of clusters of particles is analysed (formation delay, characteristic cluster size) in terms of their Stokes number and the properties of the turbulence. In addition to the criterion proposed by Fessler, Kulick & Eaton (1994) to characterize the length scale of the clusters, a new analysis is proposed to link the spray segregation with the future mixture fraction field. Once the particles have reached a dynamical equilibrium with the surrounding turbulent flow, evaporation phenomena are considered through the analysis of the mixture fraction evolution. Our goal is to observe the impact of the preferential segregation of the droplets on the mixture fraction field.

In this work, one-way coupling has been considered; with two-way coupling (Mashayek 1998; Reveillon & Vervisch 2000, 2005), the impact of the spray on the carrier phase modifies the turbulence characteristics and it becomes difficult to isolate the various interactions between dispersion, evaporation and mixing. Of course, the flow evolution considered would be more realistic, but in this paper we decided to work on simplified configurations where the main varying parameter is the droplet's Stokes number, which leads to various local segregation and mixture fraction fields. Thus, it will be possible to determine the sole impact of the spray segregation on the mixture fraction fields that are undergoing a similar turbulent mixing. Moreover,

it would not be logical to associate a realistic drag source term with an artificial turbulence forcing term in the momentum equation of the gas phase.

In the following sections, the DNS configurations and the control parameters are detailed, together with a description of the governing equations and the various hypotheses that have been used. Then, a brief description of the statistical tools is given and the various results are analysed in two stages: a preliminary description of the solid-particle dispersion and a study of the effects of the evaporation of the droplets on the mixture fraction field.

2. Governing equations and modelling

Various sets of governing equations are coupled together to carry out the computations. Because of the forcing procedure restrictions, the gas-phase velocity is evaluated in spectral space. The evolution of the mixture is described in physical space so that it can be easily coupled with the Lagrangian description of the evaporating spray.

2.1. *Gas velocity and turbulence forcing*

The gaseous carrier phase is isotropic homogeneous turbulence that is resolved in a cubic domain with periodic boundary conditions. To maintain the major properties (energy, dissipation rate, integral scale) of the spectral turbulence near to constant values, a controlled amount of energy must be transferred into the spectral simulation through a forcing procedure.

There are various ways to achieve the forcing of isotropic homogeneous turbulence in a spectral DNS. First, it is possible to freeze the magnitude of the largest structures of the spectral velocity field (Siggia & Patterson 1978; Sirovich 1991), but the stabilization of the flow parameters requires many eddy turnover times and the results are statistically dependent on the large anisotropic structures. Another solution is to use stochastic schemes (Eswaran & Pope 1988), where energy is added randomly to the low-wavenumber modes. These schemes appear to be efficient and statistically independent, but some turbulence properties fluctuated too widely around their prescribed values. A third way is to use a deterministic forcing scheme which forces the lower-wavenumber modes with a controlled amount of energy. One of the most effective such studies has been carried out by Overholt & Pope (1998). Considering the forcing methods of Kerr (1981) and Siggia & Patterson (1978), Overholt & Pope's deterministic scheme forces the simulated spectrum towards a model spectrum by using a time- and wavenumber-dependent coefficient. Recently Guichard *et al.* (2004) extended this method and proposed a fully controlled deterministic forcing scheme (FC-DFS) with a more efficient convergence rate towards the model spectrum; this reduced the fluctuations of the prescribed properties drastically. The FC-DFS scheme has been used in this work.

Turbulence is forced by adding a linear source term to the balance equation for the velocity field $\widehat{u}$ in wavenumber space:

$$\frac{\partial \widehat{u}}{\partial t} = \widehat{a} + \frac{f_\kappa}{\tau_f} \widehat{u}, \tag{2.1}$$

where $\widehat{a}$ represents the classical Navier–Stokes contributions for an incompressible flow. The forcing function $f_\kappa(\kappa_F, \Delta\kappa_F)$ is real and depends on both time t and wavenumber magnitude κ. The principle of the model is to relax the simulated spectrum E_s towards a model spectrum E_m only for a given range of low wavenumbers

($\kappa < \kappa_F$). This method has been detailed and tested Guichard *et al.* (2004); however, as all the simulations are based on this forcing procedure a brief description is given in the following.

With the new source term (2.1), the time evolution of the simulated energy spectrum E_s may be written

$$\frac{dE_s}{dt} = C_\kappa + 2\frac{f_\kappa}{\tau_f}E_s, \tag{2.2}$$

where C_κ represents the usual energy contributions without any source term. The objective is to 'attract' the simulated spectrum E_s towards a model spectrum E_m. This may be done by inserting an attraction parameter directly in the equation of the time evolution of the energy spectrum:

$$\frac{dE_s}{dt} = C_\kappa + F_\kappa \frac{\alpha_f(t)E_m(\kappa) - E_s(\kappa, t)}{\tau_f}, \tag{2.3}$$

where F_κ is a filter function varying from zero to unity:

$$F_\kappa = \frac{1 - \exp\left(-\dfrac{(\kappa - \kappa_f)^2}{\Delta\kappa^2}\right)}{1 - \exp\left(-\dfrac{\kappa_f^2}{\Delta\kappa^2}\right)} H(\kappa_f - \kappa), \tag{2.4}$$

which determines the amplitude of the forcing for every wavenumber. $H(x)$ is the Heavyside function defined by $H(x) = 1$ if $x > 0$ and $H(x) = 0$ if $x < 0$. The filter function allows a smooth transition between the relaxed and the non-relaxed zones; τ_f is a characteristic relaxation delay of the simulated spectrum E_s towards a model spectrum E_m. To keep the system stable, τ_f must be smaller than the smallest time scale of the flow (Overholt & Pope 1998). The Kolmogorov time scale

$$\tau_\kappa = \sqrt{\frac{\nu}{\langle\varepsilon\rangle}} \tag{2.5}$$

has thus been used with the following definition: $\tau_f = C_f\tau_\kappa$, where C_f is a constant coefficient (set to 0.5 in our simulations), ν is the fluid viscosity and $\langle\varepsilon\rangle$ is the current mean dissipation, determined over the whole spectral domain.

Note that, to maintain the simulated integral length scale in the vicinity of the modelled one while letting the inertial range evolve freely, the cutoff (κ_f) has to be selected at the 'beginning' of the inertial range. By identifying equation (2.2) with equation (2.3), the forcing function f_κ may be directly defined by the following expression:

$$E_s(\kappa, t)f_\kappa = \tfrac{1}{2}F_\kappa(\alpha_f(t)E_m(\kappa) - E_s(\kappa, t)). \tag{2.6}$$

The coefficient α_f controls the evolution of the mean turbulent energy $\langle k \rangle$ in the spectral domain. This is achieved by assuming the following arbitrary evolution:

$$\frac{d\langle k \rangle}{dt} = \frac{k_\infty - \langle k \rangle}{\tau_f}. \tag{2.7}$$

For simplicity, it is assumed that the target value (k_∞) corresponds to the energy of the model spectrum:

$$k_\infty = \int_\kappa E_m(\kappa)\,d\kappa. \tag{2.8}$$

To determine α_f, equation (2.7) is compared with the theoretical definition of the mean kinetic energy, which is obtained by integrating (2.2):

$$\frac{\mathrm{d}\langle k \rangle}{\mathrm{d}t} = -\langle \varepsilon \rangle + \frac{2}{\tau_f} \int_\kappa f_\kappa E_s(\kappa, t)\, \mathrm{d}\kappa. \tag{2.9}$$

By integrating equation (2.6) over κ and introducing relations (2.7) and (2.9), an expression for α_f may be derived:

$$\alpha_f(t) = \frac{k_\infty - \langle k \rangle + \tau_f \langle \varepsilon \rangle + \displaystyle\int_\kappa F_\kappa E_s(\kappa, t)\, \mathrm{d}\kappa}{\displaystyle\int_\kappa F_\kappa E_m(\kappa)\, \mathrm{d}\kappa}. \tag{2.10}$$

The forcing function f_k is obtained with the following equation:

$$f_\kappa = \frac{F_\kappa}{2E_s(\kappa, t)}\left(\alpha_f(t) E_m(\kappa) - E_s(\kappa, t) \right), \tag{2.11}$$

which allows the simulated spectrum to be attached towards the shape of a model spectrum and control of the mean kinetic energy.

2.2. *Scalar transport*

Because of the constraints of the forcing procedure, a spectral solver is used to describe the evolution of the turbulent velocity of the flow. A one-way momentum coupling determines the droplet motion. A two-way coupling could be used, although there would be no point in associating it with the artificial forcing term of the turbulence. Moreover, this one-way coupling allows us to compare the preferential segregation of various sprays in exactly the same turbulent flow.

On the other hand, to study the evolution of the mixture fraction released by the droplet evaporation, a two-way coupling is considered from the mass exchange point of view. The time evolution of species mass fractions is thus considered in physical space to simplify their coupling with the dispersed phase.

The following classical relation applies for the vapour mass fraction:

$$\frac{\partial Y_F}{\partial t} + \frac{\partial u_i Y_F}{\partial x_i} = D\frac{\partial^2 Y_F}{\partial x_i^2} + \frac{1}{\rho}\dot{\omega}_v \tag{2.12}$$

where D is the species diffusion coefficient and $\dot{\omega}_v$ the mass source term due to the evaporation of the dispersed liquid phase. A similar equation without a source term is considered for the carryier gas mass fraction: Y_O. The velocity components u_i are obtained from an inverse Fourier transform of the spectral velocity field: $u_i = TF^{-1}(\widehat{u})$.

These equations are solved with the third-order Runge–Kutta procedure already used for the spectral space. Similar sub time steps are applied for both spectral and physical solvers. A sixth-order Pade scheme from Lele (1992) allows the spatial derivatives to be determined. As for the spectral velocity field, periodic boundary conditions have been used.

2.3. *Liquid phase dispersion*

A discrete Lagrangian approach is adopted to follow the spray evolution within the gaseous oxidizer. By denoting the velocity and position vectors of every droplet k as

v_k and x_k, the relations

$$\frac{\mathrm{d}v_k}{\mathrm{d}t} = \frac{1}{\beta_k^{(v)}}(u(x_k, t) - v_k), \tag{2.13}$$

$$\frac{\mathrm{d}x_k}{\mathrm{d}t} = v_k, \tag{2.14}$$

are used to track the evolution of the spherical droplets throughout the computational domain. The vector u represents the gas velocity at the droplet position x_k. The right-hand-side term of equation (2.13) stands for a drag force applied to the droplet, where $\beta_k^{(v)}$ is a kinetic relaxation time:

$$\beta_k^{(v)} = \frac{a_k^2}{a_0^2}\frac{\tau_p}{C_k}; \tag{2.15}$$

a_k is the diameter of the droplet k and a_0 is the initial diameter of any droplet of the initially monodispersed spray. The characteristic kinetic time τ_p is defined by the relation

$$\tau_p = \frac{\rho_d a_0^2}{18\mu}, \tag{2.16}$$

and a corrective coefficient $C_k = 1 + Re_k^{2/3}/6$ (Crowe, Sommerfeld & Tsuji 1998) is introduced to allow for the variation of the drag factor according to the value of the droplet's Reynolds number $Re_k = \rho|u(x_k, t) - v_k|a_k/\mu$. These relations, assuming a spherical shape, are valid in the framework of small Weber numbers. This hypothesis is valid in all the simulations.

The evaporation of every droplet in the flow accounts for the fuel mass fraction at the droplet surface Y_k^s and the local vapour level at the droplet position, $Y_F(x_k)$. Saturation conditions mainly depend on the properties of the flow at the droplet's surface: temperature, pressure. In our simplified configuration, a constant saturation level such as $Y_k^s = Y^s$ is considered.

The following relation may be written for the surface evolution of every droplet k:

$$\frac{\mathrm{d}a_k^2}{\mathrm{d}t} = -\frac{a_k^2}{\beta_k^{(a)}}. \tag{2.17}$$

A classical model (d-square law) is to consider $\beta_k^{(a)} = $ const. It leads to a linear relation between droplet surface and time. However, in our simulation, saturation is accounted for and the characteristic relaxation time is defined by

$$\beta_k^{(a)} = \frac{Sc}{4Sh_c}\frac{\rho_d}{\mu}\frac{a_k^2}{\ln((1 - Y_F)/(1 - Y^s))}, \tag{2.18}$$

where $Sc = 0.7$ is the Schmidt number and Sh_c the convective Sherwood number, which is equal to 2 in a quiescent atmosphere; however, a correction must be applied in a convective environment. In this context, the empirical expression of Faeth and Fendell (Kuo 1986) has been used:

$$(Sh_c)_k = 2 + \frac{0.55Re_k Sc}{(1.232 + Re_k Sc^{4/3})^{1/2}}. \tag{2.19}$$

The mean evaporation delay is controlled by selecting an appropriate value for the saturation level Y^s. Usually, the evaporation delay is defined as the time necessary for a droplet to be vaporized, assuming that the mass fraction of vapour far from the
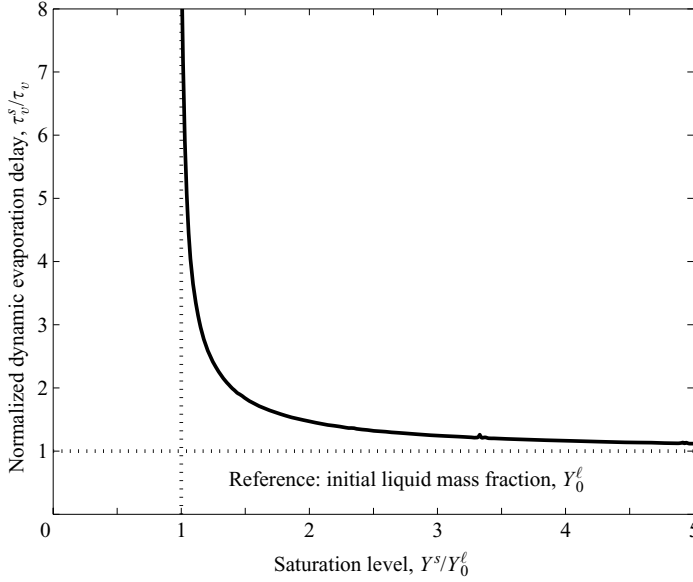
FIGURE 2. Evolution of the ratio τ_v^s/τ_v versus the saturation value of the mixture fraction Y^s. The dynamic delay τ_v^s accounts for saturation phenomena while evaporation takes place. τ_v is the classical d-square-law evaporation delay in which the surrounding vapour is not taken into account.

droplet is constant. If this mass fraction of vapour is $Y_F = 0$, the vaporization time is

$$\tau_v = \frac{Sc}{4Sh_c}\frac{\rho_d}{\mu}\frac{a_0^2}{\ln(1/(1-Y^s))}. \tag{2.20}$$

However, when saturation laws apply, it is possible to compute a dynamic characteristic evaporation delay τ_v^s of a droplet in a quiescent atmosphere that takes into account the varying level of fuel vapour around the liquid. Figure 2 shows the evolution of the ratio τ_v^s/τ_v versus the saturation level Y^s for a given initial mass fraction of liquid Y_0^l. Such an effect can be important for the evaporation of liquid fuel since generally the saturation value is low as the temperature of the atomized liquid is far from boiling temperature.

2.4. *Coupling term*

The mass source term $\dot{\omega}_v$ affects the mixture fraction evolution owing to the distribution of the Lagrangian mass on the Eulerian grid. Every droplet has mass source terms to be distributed over the Eulerian nodes and the organization of an accurate projection of those Lagrangian sources to the Eulerian mesh is not straightforward. In a real spray flow, this distribution is not instantaneous and further assumptions are needed. In our simulations, each Lagrangian source is distributed over Eulerian nodes directly surrounding the droplet. A finite volume approach is applied by considering the intersection of the elementary volume centred around the droplet and the elementary volume centred around each node (figure 3). This induces a numerical dispersion that remains weak because of the small size of the DNS grid and the small turbulent Reynolds number (Reveillon & Vervisch 2000).

For every Eulerian node, a control volume $\mathscr{V}$ is defined by the mid-distance between the neighbour nodes. Because an isotropic Cartesian grid has been used
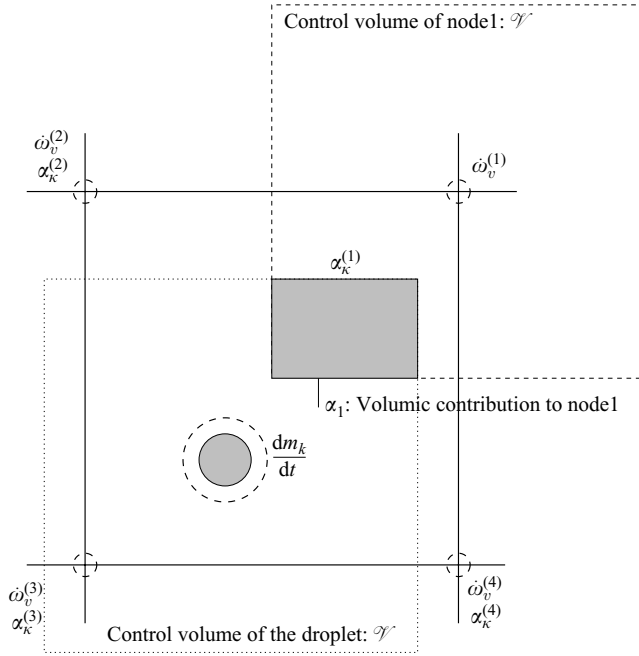
FIGURE 3. Two dimensional Sketch of the repartition of droplet source terms on the closest Eulerian nodes. A three-dimensional repartition is done in the simulations.

$(\Delta = x_{i+1} - x_i = \Delta_x = \Delta_y = \Delta_z)$, the volume $\mathscr{V}$ is defined by $\mathscr{V} = \Delta^3$. The mass source term applied to any Eulerian node n is denoted $\dot{\omega}_v^{(n)}$:

$$\dot{\omega}_v^{(n)} = \frac{1}{\mathscr{V}} \sum_k -\alpha_k^{(n)} \frac{\mathrm{d}m_k}{\mathrm{d}t}, \qquad (2.21)$$

where $\sum_k$ is the sum over all the droplets affecting the node n. $\alpha_k^{(n)}$ is the distribution coefficient of the source term of droplet k on the node n. Considering all the nodes affected the droplet k, it is necessary to have $\sum_n \alpha_k^{(n)} = 1$ to conserve mass, momentum and energy during the Lagrangian/Eulerian coupling. In fact, $\alpha_k^{(n)}$ is the portion of the control volume of node n intersecting the control volume of droplet k (figure 3):

$$\alpha_k^{(n)} = \frac{1}{\mathscr{V}} \prod_{i=1}^{3} \left(\Delta - \left| x_i^{(n)} - x_{ki} \right| \right), \qquad (2.22)$$

where $x_i^{(n)}$ and x_{ki} are the coordinates along the ith direction of node n and droplet k respectively.

The mass of droplet k in the neighbourhood of the node is defined by $m_k = \rho_d \pi a_k^3 / 6$ and, using equations (2.17) and (2.21), one may write

$$\dot{\omega}_v^{(n)} = \rho_d \frac{\pi}{4} \frac{1}{\mathscr{V}} \sum_k \alpha_k^{(n)} a_k^3 / \beta_k^{(a)}. \qquad (2.23)$$

3. Configurations and statistical considerations

The following three-stage procedure has been employed to analyse all the interactions between the turbulent flow and the dispersed phase. Vorticity contours
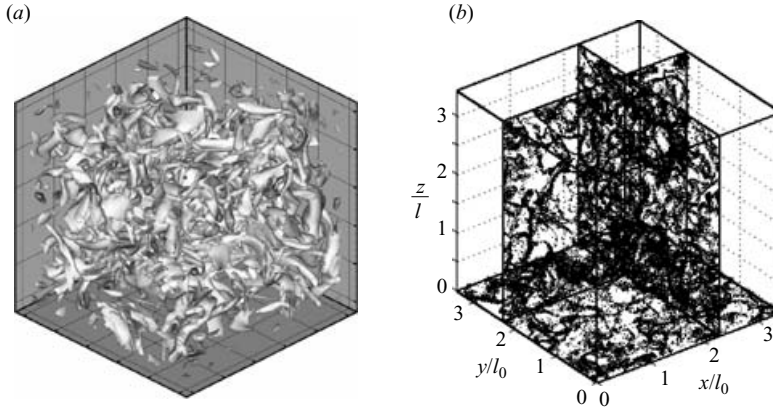
FIGURE 4. Examples of (*a*) vorticity contours and (*b*) spray dispersion.

and dispersing particles are plotted in figure 4 to illustrate both Eulerian and Lagrangian resolutions.

Stage 1: statistically stationary turbulence

In this preliminary stage, the turbulent gaseous phase evolves alone in a 129^3 Cartesian grid until its statistical properties reach a steady state thanks to the forcing procedure that keeps the mean kinetic energy $k = 3.375\,\mathrm{m^2/s^{-2}}$ at the prescribed level (figure 5(*a*)i). The mean dissipation rate ε is not specifically a prescribed parameter but it must reach a steady state ($\varepsilon = 2.75\times10^4\,\mathrm{m^2/s^{-3}}$), as shown in figure 5(*a*)(iii). The energy spectrum allows us to determine a reference wavenumber κ_0 corresponding to turbulence scales that contain most of the kinetic energy. The corresponding physical length $l_0 = 2\pi/\kappa_0$ is an integral scale of the flow that has been used as a reference parameter in this work along with its spectral counterpart κ_0. In all the simulations, $\kappa_0 = 7\Delta\kappa$, where $\Delta\kappa$ is the spectral grid size defined by $\Delta\kappa = 2\pi/L$ and L is the cubical domain dimension equal to 3 mm. The maximum energy length l_0 is thus equal to $L/7$ and remains constant as shown in figure 5(*a*)(ii). The velocity root-mean-square, $u' = 1.5\,\mathrm{m\,s^{-1}}$, is used as reference parameter along with the eddy turnover time $\tau_0 = l_0/u'$ and the characteristic time τ_κ of the velocity fluctuations of the smallest structures ($\eta \approx 1.8 \times 10^{-5}$ m). The turbulent Reynolds number of the simulation is $Re_{l_0} = 43$ and the parameters of the filter function, as defined by Guichard *et al.* (2004), are $\kappa_F = 9\,\Delta\kappa$ and $\Delta\kappa_F = 3\,\Delta\kappa$.

Stage 2: spray dynamical equilibrium

Several eddy turnover times after the turbulent flow reaches its stationary state, $N_d \approx 2\,150\,000$ mono-dispersed non-evaporating particles are randomly embedded throughout the computational domain with a zero initial velocity. The drag force, described above in equation (2.13), sets particles in motion. Then, the spray reaches a dynamical equilibrium with the turbulence (figure 4*b*). It corresponds to a stationary slip velocity standard deviation. Droplet dispersion is usually characterized by the Stokes number $St = \tau_p/\tau_\kappa$ (Wang & Maxey 1993), which indicates the ability of droplets to capture local variations of the carrier-phase velocity. Turbulence properties being fixed, simulations were carried out by modifying the τ_p parameter. By doing so, 12 Stokes numbers varying between 0.025 and 11 were considered.

To characterize droplet dispersion and preferential concentration, a density $\xi(\boldsymbol{x}, t)$, describing the local mass of liquid per unit of volume has been defined. To make
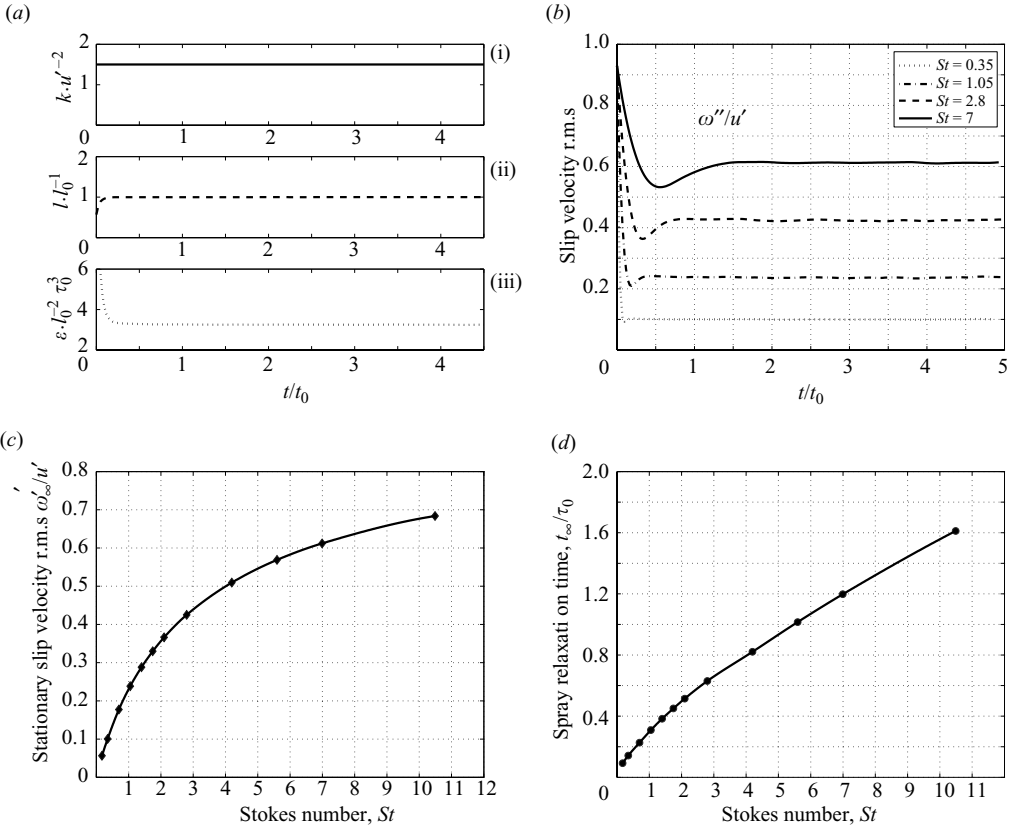
FIGURE 5. Statistically stationary convergence of turbulence and spray properties. (*a*) time evolution of the normalized; (i) kinetic energy k, (ii) maximum energy length scale l_0, and (iii) dissipation ε; (*b*) time evolution of particle slip velocity r.m.s. (w''); (*c*) final ($t > t_\infty$) stationary level of particle slip velocity r.m.s. (w''_∞); (*d*) spray relaxation time (t_∞) necessary for the spray to be in equilibrium with the turbulent carrier phase.

the spectral analysis of physical properties easier, a Eulerian computational grid was used and $\xi(\boldsymbol{x}, t)$ is determined by considering the droplets accumulated around each node. A mean reference mass density is defined by $\bar{\xi}_0 = m_d N_d/L^3$ where m_d is the initial mass of each droplet (mono-dispersed spray). The constant parameter $\bar{\xi}_0$ is used to normalize the evolution of $\xi(\boldsymbol{x}, t)$. Thus, in a non-evaporating mode, $\xi(\boldsymbol{x}, t)/\bar{\xi}_0$, which may also be considered as a number density, has a constant unity mean $\bar{\xi}(t) = L^{-3} \int \xi(\boldsymbol{x}, t) \, \mathrm{d}\boldsymbol{x} = \bar{\xi}_0$ over the whole domain and its standard deviation $\xi'(t) = L^{-3}(\int(\xi(\boldsymbol{x}, t) - \bar{\xi}(t))^2 \, \mathrm{d}\boldsymbol{x})^{(1/2)}$, normalized by $\bar{\xi}_0$ in the following, identifies the droplet segregation level. Note that, in the following, an ovebar stands for the mean over the Eulerian grid whereas a tilde denotes is the mean over the Lagrangian particles or droplets.

Stage 3: liquid phase evaporation and micro-mixing

When the droplets are evaporating, $\bar{\xi}/\bar{\xi}_0$ is bounded between 1 and 0. $\bar{\xi}/\bar{\xi}_0$ provides information about the evaporation state whereas $\xi'/\bar{\xi}$ characterizes the droplet segregation. Using the parameter ξ to characterize the spray evolution and preferential segregation is not the usual choice in other work on preferential segregation in sprays, but it allows well-established results to be retrieved (Fessler *et al.* 1994). The method

was chosen in accordance with the main objective of this paper, which is to analyse the correlations between the droplet concentration and the micro-mixing of the gaseous fuel released by the liquid evaporation. Using a Eulerian droplet density allows a direct comparison with the Eulerian mixture fraction field Z. In the last stage, once the particles have reached a dynamical equilibrium with the surrounding turbulence, they are allowed to evaporate according to a specific characteristic evaporation delay τ_v prescribed by setting the saturation level as described above. Thus, for a given initial non-evaporating configuration, various simulations with different evaporation delays will be carried out and analysed.

To describe the mixing between the gaseous fuel and the oxidizer, the usual definition of the mixture fraction Z is chosen (Linán & Williams 1993; Poinsot & Veynante 2001) leading to $Z = Y_F$ in an inert flow. A passive scalar is defined as $\varphi = s_r Y_F - Y_O$ (Linán & Williams 1993), where the stoichiometric mass ratio is $s_r = 11$ when considering the single-step reaction $C_7H_{16} + 11O_2 \rightarrow 7CO_2 + 8H_2O$. Normalizing φ yields the mixture fraction $Z = (\Phi_o(Y_F/Y_{F,o}) - (Y_O/Y_{O,o}) + 1)/(\Phi_o + 1)$, with $Y_{F,o} = 1$, $Y_{O,o} = 0.23$ and $\Phi_o = s_r Y_{F,o}/Y_{O,o}$, where subscript o denotes fresh gases dilution. Note that in the case of spray evaporation, Z cannot reach unity, but a local maximum level depending on saturation conditions. Consequently, a normalization of Z is introduced by using the saturation limit Z_s. Z/Z_s is thus bounded between 0 and 1 and it is of practical interest for analysing correlations between the evaporating spray and the turbulent mixing.

4. Results and discussion

Although homogeneous turbulence is a straightforward configuration, the addition of an evaporating dispersed phase introduces many poorly understood interactions between turbulence, spray, mixing and combustion. As described in the introduction, for clarity this paper focuses on the correlations between the mixture fraction field and the preferential droplet segregation. The analysis of flame ignition and propagation or model closures will be the purpose of future work. In the first part of this section, the equilibrium regimes of non-evaporating droplets before evaporation takes place are depicted. Then evaporation is considered using both a liquid and a gas analysis. In particular, the evolution of the mixture fraction PDF is studied. Finally, the topologies of the liquid and vapour fields are investigated using a spectral analysis.

4.1. *Liquid dispersion*

The equilibrium of the spray with its surrounding carrier phase is detected through the Lagrangian statistics of the slip velocity $\boldsymbol{w}_k = (\boldsymbol{u}t(\boldsymbol{x}_k, t) - \boldsymbol{v}_k)$, where $\boldsymbol{u}$ is the gas velocity at the droplet location and $\boldsymbol{v}$ is the droplet velocity. Because of the homogeneous nature of the turbulence and the dispersion, the mean value of the slip velocity, defined by $\tilde{\boldsymbol{w}} = N_d^{-1} \sum_{k=1}^{N_d} \boldsymbol{w}_k$, remains equal to zero. However, as shown in figure 5(*b*), the slip velocity root mean square $w'' = \sqrt{\overline{w_i w_i}}$ evolves toward a stationary value w''_∞ corresponding to the equilibrium of the spray with the surrounding gas. Because particles are initially randomly distributed in the computational domain with a zero velocity, w''/u' is unity at time $t = 0$; u' stands for the r.m.s. of the gas velocity, sampled with the initial field of particles. Then, as described previously, the drag forces set the particles in motion and, depending on the Stokes number, w'' reaches a steady state in less than $0.1\tau_0$ (figure 5*d*) for a small Stokes number ($St = 0.35$) whereas $1.6\tau_0$ is needed for the largest value of the Stokes number ($St = 11$). This is an important point because, in more complex configurations like combustion chambers,

even though evaporation and ignition delays are short, droplets are most certainly already in dynamical equilibrium when evaporation takes place. The final mean stationary value of the slip velocity standard deviation, w''_∞, is in plotted figure 5(*c*) with respect to the droplet's Stokes number. This value is zero when the droplets are small enough to follow all the velocity fluctuations of the flow, and it increases regularly to reach the value one asymptotically, corresponding to droplets that are too heavy to move ($St = \infty$).

To study the preferential concentration of discrete particles in turbulent flows, several approaches exist: see for instance Squires & Eaton (1991), Wang & Maxey (1993), Fessler *et al.* (1994), Simonin, Fevrier & Laviéville (1993) and Aliseda *et al.* (2002). If a statistically homogenously distributed spray is randomly injected, i.e. if there is no preferential segregation, the distribution of the number of particles per control volume (CV) of a given size must follow a binomial distribution, which may be approximated by a Poisson distribution in our configurations. Hence, the study of the preferential concentration is usually based (Fessler *et al.* 1994) on the difference between the actual segregated distribution and the Poisson distribution. It is characterized by

$$\Sigma = (\sigma - \sqrt{\lambda})/\lambda, \tag{4.1}$$

where λ is the average number of particles per cell whereas σ and $\sqrt{\lambda}$ are the standard deviations of the particle distribution and the Poisson distribution, respectively. For a given Lagrangian distribution of the particles, Σ depends strongly on the size of the CV considered. However, according to Fessler *et al.* (1994), the length scale corresponding to the characteristic cluster size is to $\Delta_{\Sigma max}$, which is the size of the CV when Σ reaches a maximum value.

In the case considered in this work, the particles are liquid droplets of fuel that are evaporated to prepare the reactive mixture. Preferential concentrations of particles are potentially important when describing induced heterogeneities that could appear in the mixture fraction field. Therefore, another parameter, more representative of the evaporation and turbulent mixing processes, has been considered to describe preferential segregation effects.

Droplet dispersion and preferential segregation have been analysed from a Eulerian point of view using the local Eulerian liquid density $\xi(x, t)$. Instantaneous fields of ξ are plotted in figure 6(*b–d*) for three Stokes numbers ($St = 0.17$, $St = 1.05$ and $St = 5.6$) along with the corresponding vorticity field (figure 6*a*). These four fields have been captured at exactly the same time after droplet dispersion has reached a stationary value ($t > t_\infty$). Even without any quantitative analysis, it is possible to see the dramatic impact of the particles' inertia on their dispersion properties; even with a small Stokes number, particles tend to leave the vortex cores and segregate in weak vorticity areas. This phenomenon may be seen in figures 6(*b*) and 6(*c*) where ξ is shown for $St = 0.17$ and $St = 1.05$, respectively. This last case shows a normalized liquid density $\xi/\bar{\xi}_0$ between 0 (no droplets) and 5 (five times the mean density). As will be shown later, density fluctuations reach a maximum when $St = 1$. When $St = 0.17$, segregation is already clearly visible (maximum deviation: 2.5) although there are more intermediate-density areas (figure 6*b*). When the $St = 1$ limit is exceeded, the droplet distribution tends to be completely different than for $St \leqslant 1$, see figure 6(*d*): kinetic times become large enough for the droplets to cross high-vorticity areas, leading to a less segregated spray (maximum deviation: 2.5). This result is confirmed in figure 7 where the mean liquid density conditioned by the local vorticity level is plotted for various Stokes numbers. For highly segregated sprays
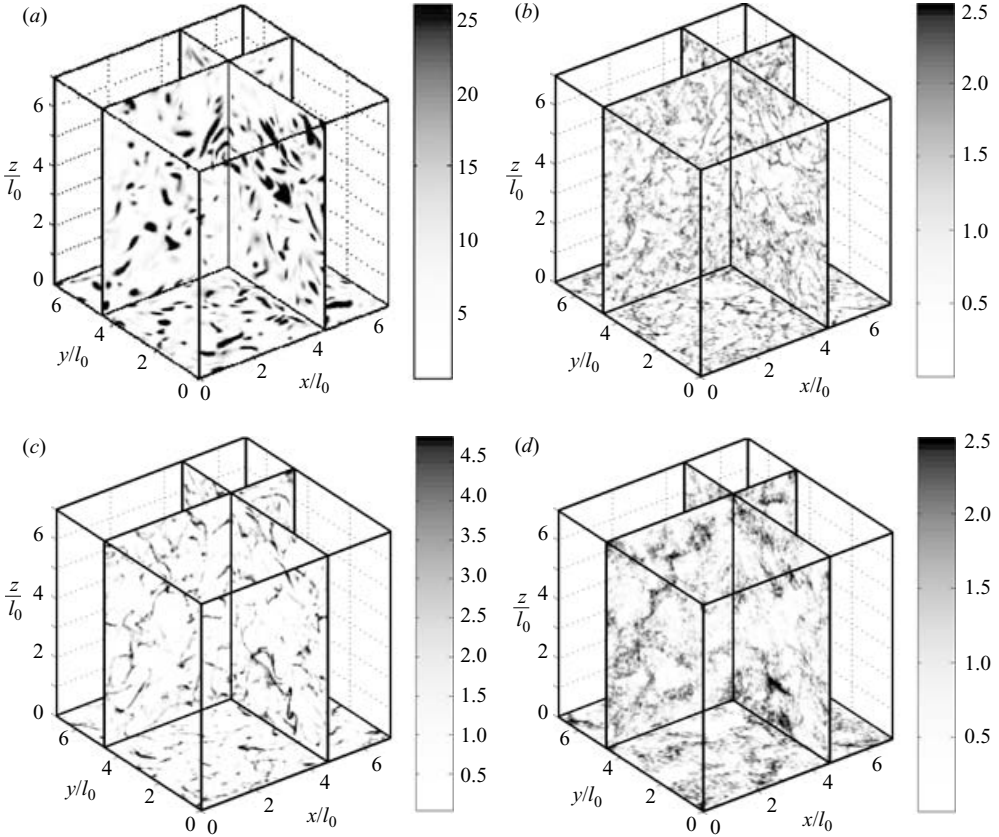
FIGURE 6. (*a*) Carrier-phase vorticity $\tau_0 \sqrt{\omega^2}$; spray concentration areas $\xi/\bar{\xi}_0$ for (*b*) $St = 0.17$, (*c*) $St = 1.05$, (*d*) $St = 5.6$.

($St = 1.05$), high-vorticity areas are almost empty, with an average value of $\bar{\xi}/\bar{\xi}_0$ equal to 0.2, whereas when vorticity tends to 0, $\bar{\xi}/\bar{\xi}_0$ converges towards 2. Figure 7 is in accordance with classical results such as the work of Squires & Eaton (1991). They found a maximum correlation between the number of particles and the vorticity level for a Stokes number equal to 0.15. However, they used a Stokes number based on the integral time scale of the turbulence. On swapping it by the Kolmogorov time scale, the peak correlation occurs for a unity Stokes number. The Kolmogorov scaling is necessary to characterize segregation effect, as outlined by Wang & Maxey (1993). When $St = 0.17$ and $St = 5.6$ the correlation between low-vorticity areas and high-droplet-density clusters is less pronounced. However, because of the ballistic nature of the heavy droplets ($St = 5.6$) the high-vorticity areas are still densely populated. This confirms the qualitative result of figure 6(*d*).

To evaluate the preferential segregation of the droplets embedded in the turbulent flow, ξ'_∞ is plotted in figure 8(*a*). This parameter is the standard deviation of the field ξ when droplets are in dynamical equilibrium with the carrier phase ($t > t_\infty$). Starting from $St = 0.025$ with $\xi'_\infty/\bar{\xi}_0 = 0.55$, a maximum segregation $\xi'_\infty/\bar{\xi}_0 = 1.4$ is observed for a unity Stokes number before a progressive decay. This parameter shows the characteristic liquid density level in clusters that have been formed by the turbulent structures.
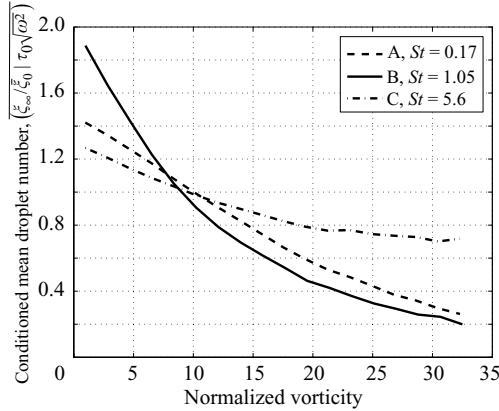
FIGURE 7. Mean value of stationary droplet number ξ_∞/ξ_0 conditioned by the carrier-phase vorticity level ω.
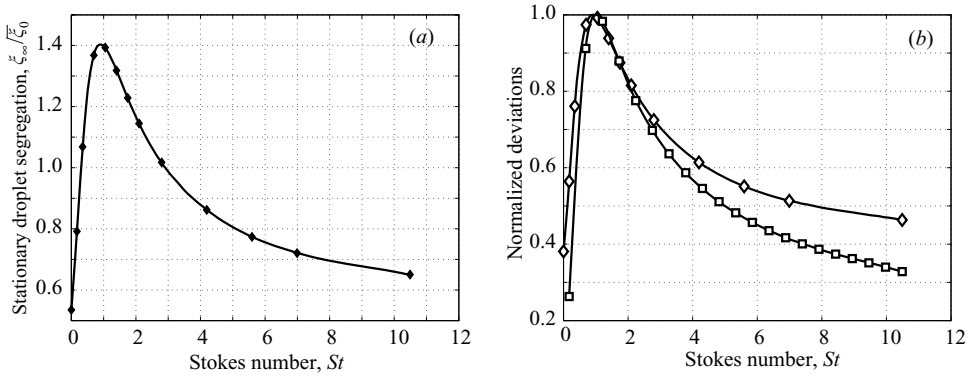

FIGURE 8. (*a*) Final stationary values of the droplet segregation parameter ξ'_∞ normalized by the initial mean value of $\xi : \overline{\xi}_0$. (*b*) Normalized standard deviations. Squares: deviation from a Poisson distribution Σ, diamonds: droplet segregation parameter ξ'_∞.

The variable ξ is not classically used to capture the properties of dispersed particles; therefore, the results have been compared in figure 8(*b*) with the maximum of Σ, which is the deviation from the Poisson distribution as defined in equation (4.1). Both Σ and ξ'_∞ being standard deviations of different variables, quantitative comparisons are not relevant in this case and the data have been normalized by their maximum value, when $St = 1$. The evolution of the deviation ξ'_∞ with respect to the Stokes number is very similar to that of the classical parameter Σ, although ξ'_∞ is slightly higher when $St > 3$. However, both curves reach a maximum value when $St = 1$. Wang & Maxey (1993) and Fessler *et al.* (1994) have shown a similar dependence of the segregation intensity on the Stokes number. This confirms that the parameter ξ defined in this work is relevant to characterize segregation.

Similarly, it is possible to determine, with various methods, the characteristic size of the clouds (or clusters) of particles. In this paper, we used the information obtained from the energy spectrum $E_\xi(\kappa)$ (figure 9) of the variable $\xi(x, t)$ when $t > t_\infty$, and then we extracted $l_\xi = 2\pi/\kappa_\xi$ where κ_ξ is the position, in spectral space, of the most energetic level. Plotting the l_ξ dependence on the Stokes number in figure 10 demonstrates the large-scale effects of the turbulence on the spray. The cluster sizes
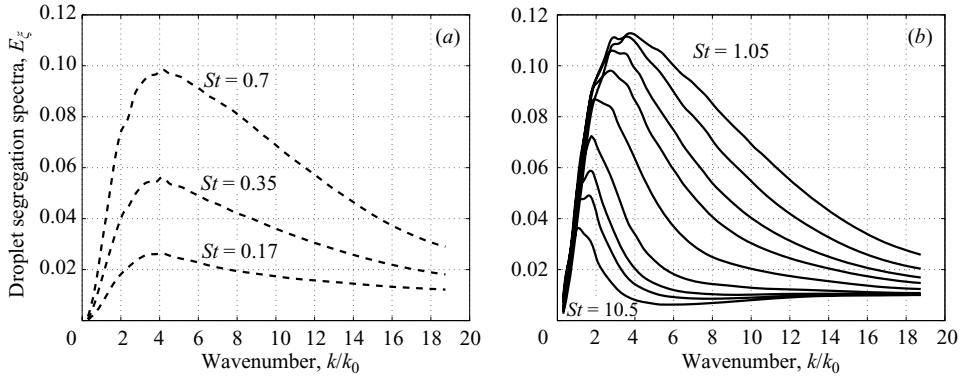
FIGURE 9. Stationary energy spectra of the droplet concentration parameter ξ for (*a*) small Stokes numbers ($St < 1$); (*b*) large Stokes numbers ($St > 1$).
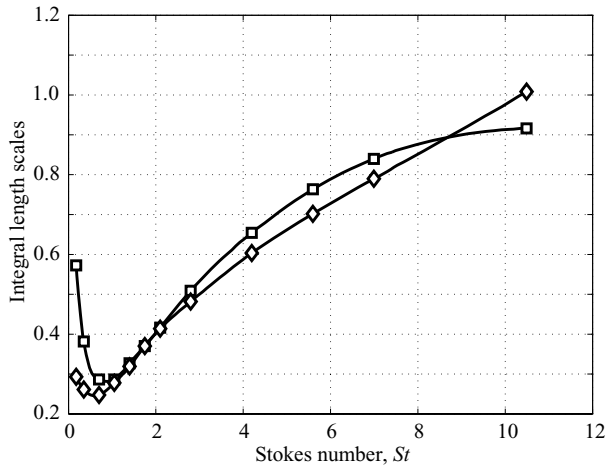

FIGURE 10. Characteristic cluster size determined with two different methods. Squares: cell size of the optimal deviation from the Poisson distribution $\Delta_{\Sigma max}$, diamonds: size of the most energetic clusters l_ξ (determined from the energy spectrum of the droplet density).

computed from E_ξ are compared (figure 10) with the ones obtained in the classical Lagrangian way by Fessler *et al.* (1994). In that approach, the cluster size denoted $\Delta_{\Sigma max}$ is the width of the CV when Σ reaches a maximum value. Both l_ξ and $\Delta_{\Sigma max}$ show a similar evolution with a minimum size for $St = 1$. In their experiment Aliseda *et al.* (2002) compared the characteristic cluster size $\Delta_{\Sigma max}$ to the length scale found using a method proposed by Wang & Maxey (1993). In that approach, the change between the actual distribution and the binomial distribution is measured as the square of the difference of probabilities given by the two distributions summed over all possible values. Aliseda *et al.* found that both methods lead to the same characteristic length scale for the cluster. Thus, using the Eulerian parameter ξ is in accordance with the classical Lagrangian approach to the analysis of preferential segregation. Notice that for the measurement of the characteristic cluster length scale, Aliseda *et al.* (2002) used all the droplet class sizes. Thus it is not possible to determine the Stokes number dependencey of the cluster's characteristic length scale. The two methods they used to find the cluster length scale agree globally when considering

all the droplet sizes. It is still possible that some difference may appear for specific values of Stokes as we found when comparing $\Delta_{\Sigma max}$ to ξ.

Fessler *et al.* (1994) conducted experiments with various sets of particles corresponding to Stokes numbers ranging from 1.7 up to 130. Their study does not extend to Stokes numbers smaller than unity. It appears that $\Delta_{\Sigma max}$ is dependent on the Stokes number: starting with a value of the order of the Kolmogorov length scale, it increases as the Stokes number increases. For Stokes number greater than unity, the parameter ξ this trend recovers. In our DNS, when $St < 1$, the evolution of the cluster size obtained with both Σ and ξ is similar although the length scales are different (figure 10). However, using ξ as reference parameter offers a new range of possible analyses, developed below.

From a phenomenological point of view, the cluster size evolution results from the competition between three physical phenomena: the ejection of the droplets from the vortex cores by the turbulence, the turbulent micro-mixing (prevalent when $St < 1$) and the ballistic effects (prevalent when $St > 1$). Droplets tend to be ejected from the turbulent structures to form clusters concentrated in low-vorticity areas. However, for droplets with a small Stokes number, turbulent micro-mixing counteracts the segregation process and 'diffuse' clouds are obtained (as seen in figure 6b): the lighter the droplets, the more effective the mixing and the larger the characteristic size of the cluster. When $St = 1$, an optimal segregation is obtained because micro-mixing is weak and the droplets are not heavy enough to leave low-vorticity areas where they are trapped. However, as soon as inertia is prevalent ($St > 1$) the particles are able to cross turbulent structures no matter what their vorticity is and the characteristic size of the clusters increases again. In figure 10, it is clear that both l_ξ and $\Delta_{\Sigma max}$ capture this natural dependence on the Stokes number.

To conclude on the non-evaporating dispersion aspect, our results show that preferential segregation in sprays cannot be characterized using only the mean segregation parameter ξ'_∞ and the mean density $\bar{\xi}$. For two sprays with the same mean density and with Stokes numbers of 0.17 and 5.6, a similar mean segregation level 0.85 is found in figure 8(a). However, the corresponding topologies of spray density are distinct, as may be seen in figures 6(b) and 6(d) where ξ is plotted for $St = 0.17$ and $St = 5.6$, respectively. This dramatic difference is confirmed in figure 10 by the characteristic sizes of the clusters of particles being equal to 0.29 and 0.65 when normalized by the characteristic length scale of the most energetic turbulent structures l_0. Consequently, for two fields with identical first moments of ξ, different mixture fraction topologies can be obtained from droplet evaporation and different combustion regimes might be observed if the ignition delay is short compared to the turbulent mixing time. Thus, in addition to $\bar{\xi}$ and ξ'_∞, a third parameter, which depends on the droplet's Stokes number, is necessary to describe accurately the preferential segregation of the spray and the subsequent mixture fraction field.

4.2. *Evaporation and turbulent mixing*

Once dynamical equilibrium is reached between the turbulent gaseous flow and the dispersed phase, evaporation is activated. Mixing between the fuel vapour and the gaseous oxidizer is characterized by the mixture fraction Z. It is bounded between zero, when there is no vapour, and a limit value Z_s, which is the saturation level. Three cases are chosen with three different initial Stokes numbers. They are listed in table 1: cases B have a Stokes number close to unity when segregation is maximum, cases A and C correspond to low and high Stokes numbers, respectively. As detailed previously, their segregation parameter ξ' is the same, although the characteristic cluster size and the

	$St = 0.17$	$St = 1.05$	$St = 5.6$
$\tau_v = \infty$	A	B	C
$\tau_v = 0.5\tau_0$	A_1	B_1	C_1
$\tau_v = \tau_0$	A_2	B_2	C_2
$\tau_v = 2\tau_0$	A_3	B_3	C_3

TABLE 1. Configuration labels, St is Stokes number, τ_v is evaporation delay. Non-evaporating case: $\tau_v = \infty$.
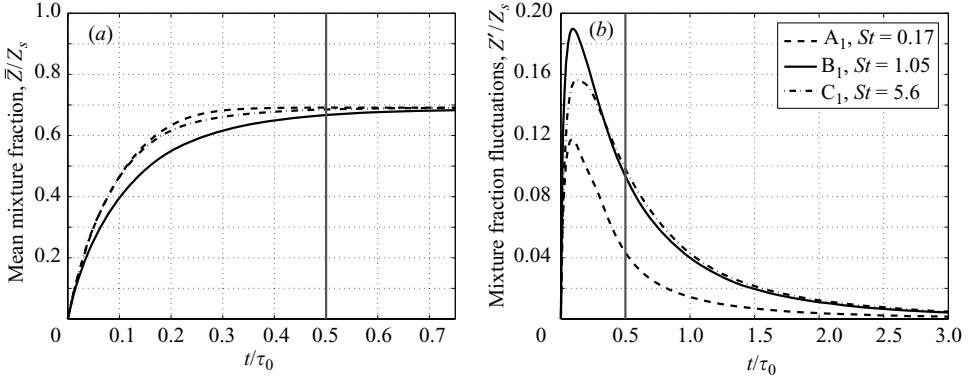
FIGURE 11. Evolution of mixture fraction statistics in the domain, characteristic evaporation time is $0.5\tau_0$: (a) mean mixture fraction, (b) deviation.

droplet dynamics are very different. Various characteristic evaporation delays τ_v have been considered: (1) $\tau_v = 0.5\tau_0$, (2) τ_0, (3) $2\tau_0$. Configuration labels are summarized in table 1 as well.

The evolution of $\overline{Z}/Z_s$ is plotted in figure 11(a) for cases A_1, B_1 and C_1. It is clear from this figure that the most segregated case (B_1, unity Stokes number) takes the longest time to evaporate although a first-order estimation (obtained from the tangent of the curve at $t/\tau_0 = 0$) would give the same results for the three cases. Note that both configurations A_1 and C_1 start with exactly the same evolution of the mean mixture fraction; the initial droplet dispersion level being the same in both cases, the evaporation rate is similar at first and only a small discrepancy, which will be explained later, appears when $t/\tau_0 = 0.2$. No matter what the Stokes number of the droplets is, the mean mixture fraction evolution depends only on the initial segregation level of the particles. If the segregation level is small enough to avoid the creation of saturated pockets of fuel vapour, whatever the dynamics (or the Stokes number) of the droplets is, the evolution of $\overline{Z}$ may be easily estimated by a classical d-square law. On the other hand, if the segregation level and mass of liquid fuel are high enough for the pocket of vapour to reach the saturation limit, the evolution of $\overline{Z}$ is affected. Clusters containing a large number density of droplets are quickly surrounded by a high level of vapour concentration. Consequently, the gaseous fuel diffusion flux from the droplet surface to the surrounding gas is reduced because of the saturation that strongly decreases the evaporation rate for each droplet embedded in any cluster. Evaporation may even stop if the vapour concentration locally reaches the saturation limit. Consequently, the droplets need more time to evaporate. Some of them, generally the heaviest ones, may be ejected from the cluster by turbulent motion
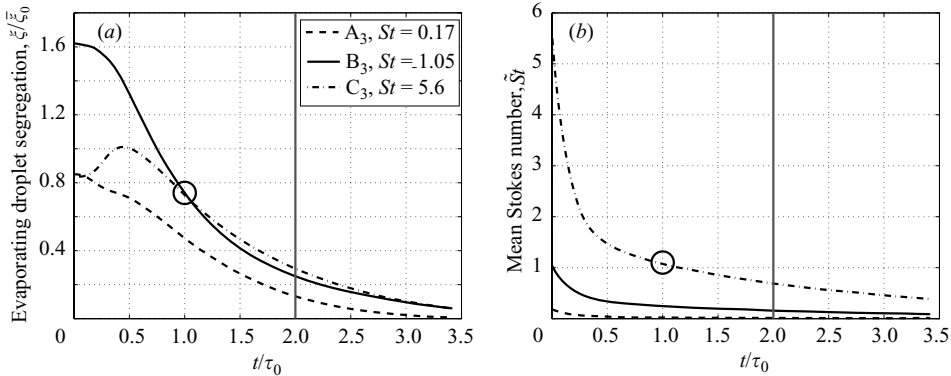
FIGURE 12. Droplet mean properties evolution, characteristic evaporation time $2\tau_0$. (a) droplet number fluctuations, (b) mean Stokes number.

to reach areas where vapour concentration is low enough for them to evaporate. On the other hand, the smallest ones may be trapped in the cluster. In that case, the driving mechanism of the evaporation is linked to the global diffusive flux of vapour from the saturated cluster towards areas with low vapour concentration.

A very different behaviour may be observed in figure 11(b) where the evolution of the standard deviation of the mixture fraction Z' is plotted for cases A_1, B_1, C_1. From a general point of view, the global shape of the curves is the same: starting from $Z'/Z_s = 0$ when evaporation begins, the curves reach a maximum value long before the characteristic evaporation delay (when $t/\tau_v \approx 0.2$). It is here that the dissipation effects on the mixture fraction fluctuations become greater than the effects of the evaporation. Consequently, the mixture fraction fluctuations decrease continuously. Details of the competition between evaporation and dissipation may be found in Reveillon & Vervisch (2000).

A more detailed analysis shows different local evolutions of the mixture fraction. First, the most segregated spray generates the most fluctuating mixture fraction field (case B_1, $St = 1.05$). Droplets are accumulated in small clusters and when evaporation starts, high levels of mixture fraction are obtained in small control volumes, leading to a strong deviation Z'. Another important point to note is the evolution of the deviation Z' of case C_1 that initially evolves like case A_1 because of the initially similar droplet segregation level. However, it very quickly exceeds (more than 30%) the maximum value of Z'_{A1} before joining, almost exactly, the curve Z'_{B1} corresponding to the highly segregated case. This behaviour, very different from that observed previously in the evolution of $\overline{Z}$, is due to the decrease of the mean Stokes number of the spray that leads to a very quick segregation of the evaporating droplets of case C_1. On the other hand, there is no change in segregation for case A_1 ($St = 0.17$) as the Stokes number becomes smaller and smaller.

This interpretation is confirmed in figure 12 where the evolution of the droplet segregation parameter ξ' and the droplets' mean Stokes number is plotted for cases A_3, B_3, C_3 ($\tau_v = 2\tau_0$), which shows this behaviour more clearly. The evolution of spray segregation represented by the standard deviation of the droplet density ξ' is shown in figure 12(a). The general trend of cases B and A is a decrease of the segregation because of the decrease of the corresponding Stokes number that may be seen in figure 12(b). The turbulent micro-mixing becomes more and more effective, leading to a less segregated spray. When the Stokes number is initially greater than
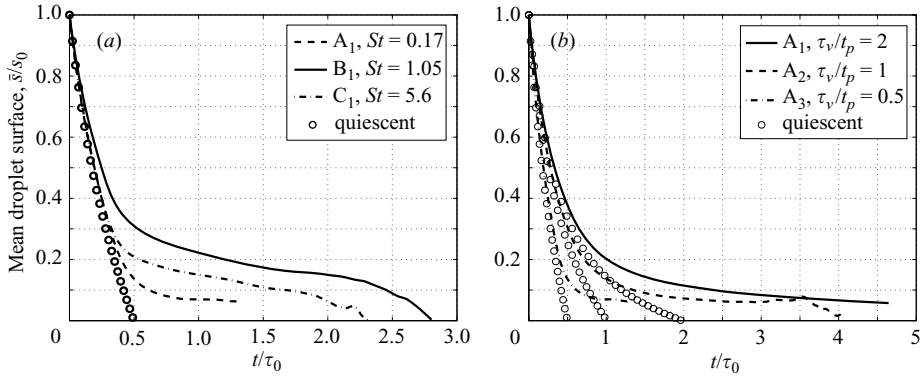
FIGURE 13. Droplet mean surface evolution. Symbols: droplet evaporation
in a quiescent atmosphere.

unity (case C) the segregation first increases before following the general decay. The
initial elevation of the segregation level corresponds to an evolution of the droplet
dynamics to a level that is more efficient (unity Stokes number) in creating clusters
and, therefore, increases ξ' momentarily. This modification of the evaporating droplet
dynamics has a direct impact on the mixture fraction evolution as seen in figure 11(*b*).
It also explains the small discrepancy between cases A and C in the evolution of
$\overline{Z}$ (figure 11*a*) underlined previously; the temporary formation of clusters in case C
leads to slightly more saturated clouds of fuel vapour. Consequently, it delays the
evaporation process.

The evolution of the mean droplet surface divided by its initial value is shown
in figure 13 for various Stokes numbers and various evaporation delays. Additional
curves, represented by circles, show the mean droplet surface evolution that would be
obtained if there were no preferential segregation (homogeneous droplet distribution).
This curve may be obtained analytically from equations (2.17) and (2.18) where Y_F
is replaced by the mean mass fraction of fuel increasing in the domain. This model
has been used to determine the characteristic evaporation delay τ_v. Figure 13(*a*)
demonstrates the dramatic effect of the segregation of the dispersed phase on the
evaporation process. Two distinct stages may be observed. First, when evaporation
starts, far from the saturation limit, the decrease in the mean droplet surface area
calculated from the DNS is similar to the results obtained with the analytical model
that neglects the segregation phenomena. Then, depending on the Stokes number (i.e.
on the droplet segregation level), a second evaporating stage may be observed with a
slower rate. This behaviour is confirmed by figure 13(*b*) where the surface evolution
has been plotted for a given Stokes number ($St = 0.17$) and various evaporation
delays.

The evaporation scenario is shown in figure 14 and may be summarized as follows:
(1) Initially the evaporation is very quick since no vapour concentration prevents
it. (2) Soon a cluster that contains a high density of droplets reaches a vapour
concentration close to saturation. Consequently, the evaporation rate of the droplets
inside the cluster is strongly diminished, if not stopped. Then, two routes are possible.
(3a) The lightest droplets are not able to leave the saturated area because of their
lack of inertia. Their evaporation rate is thus strongly related to the diffusion rate
of the pocket of vapour toward the fresh gases. In this case, all the droplets inside a
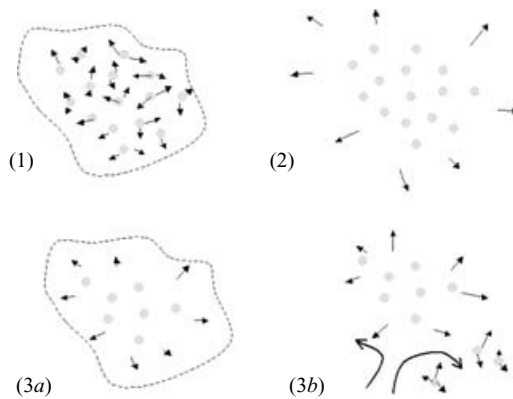cluster could be considered as a single entity, which mimics the evaporation law for a

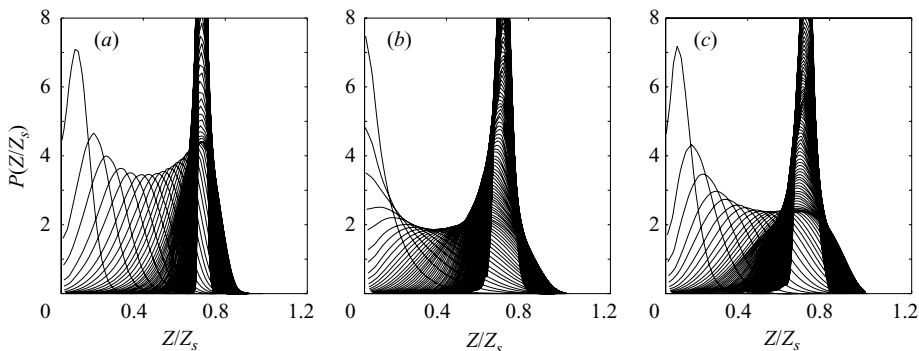FIGURE 14. Sketch of the evaporation process. Labels (1)–(3) are described in the text.

FIGURE 15. Time evolution of the PDF of Z/Z_s. 30 PDF over one characteristic evaporation time. (*a*) $St = 0.17$, (*b*) 1.05, (*c*) 5.6.

single droplet. (3b) Turbulent motion contributes to dispersing the heaviest droplets. Then, they may reach non-saturated areas to finish their evaporation process.

4.3. *Mixture fraction PDF*

There are various ways to describe the statistics of the vapour mass fraction. In the preceding section, the evolution of the first two moments of Z was plotted in figure 11 to characterize the direct impact of the droplet segregation on the corresponding mixture fraction fluctuations. A thorough statistical analysis can be carried out by detailing the transformation of $P(Z/Z_s)$, the probability density function (PDF) of the mixture fraction variable Z normalized by the saturation value Z_s. By doing so, the phase space is bounded between 0 and 1, facilitating the analysis. General time evolutions of Z/Z_s are plotted in figure 15 for the three reference Stokes numbers: $St = 0.17$, $St = 1.05$ and $St = 5.6$. Starting from a Dirac function (not represented) at $Z/Z_s = 0$ when evaporation begins, the PDF evolves, with a bell-shaped curve, towards another Dirac function corresponding to the final mean mixture fraction in the volume.

More details may be found in figure 16 where snapshots of the PDF shapes are plotted for three different times. Plot (*a*) shows the three PDFs when $t = 0.025\tau_0$. Although the mean mixture fraction is small, it is clear that the curves corresponding to $St = 0.17$ and $St = 5.6$ are similar for short times. This is a remarkable property. We already knew, from figure 8(*a*) that the segregation parameter ξ', and therefore
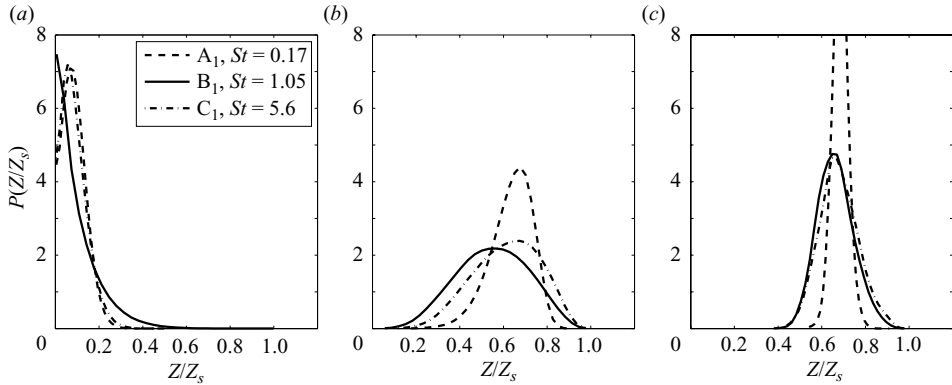
FIGURE 16. PDF of Z for various Stokes numbers: (a) $t = 0.025\tau_0$, (b) $t = 0.5\tau_0$ and (c) $t = 1.15\tau_0$.

the mixture fraction variance Z', were similar in the early stages of the evaporation for $St = 0.17$ and $St = 5.6$. However, the corresponding cluster sizes (figure 10) were different, possibly leading to different mixture fraction topologies. It appears in figure 16(a) that the PDF shape is not strongly affected by the various cluster sizes in the early stages of the evaporation process. Thus, not only are the first two moments similar but also the moments greater than two. However, numerous models are based on the first two moments of the mixture fraction variable and it is useful to note that those models, often deduced from the analysis of the mixing of a purely gaseous flow, may be used for two-phase flows if the evaporation source terms are correctly accounted for.

Figures 16(b) and 16(c) confirm the general evolution seen in figure 11(b) when the Stokes number of the heaviest droplets reaches the optimal segregation level corresponding to $St = 1$. Consequently the PDF of case C_1 relaxes toward the PDF of case B_1. At an intermediate stage (centre plot of figure 16), both $St = 0.17$ and $St = 5.6$ PDFs are still centred around a similar mean value but their shapes are no longer alike. The difference between the shapes is considerable and it is clear that combustion models based on such a PDF would give contrasting results. The last point to be noticed in figure 16(b) is that, apart from case $St = 0.17$, the PDFs are not symmetrical around the mean. Cases $St = 0.17$ and $St = 5.6$ correspond to dispersing droplets that can be found outside the pockets of vapour generated around droplet clusters because of turbulent micro-mixing or ballistic effects. This usual behaviour leads to an increased probability of finding small mixture fraction levels. At this stage it is difficult to determine if combustion would be strongly affected by this result. However, if that were the case, it would be necessary to take into account the lack in symmetry of the PDF in the models.

4.4. *Spatial distribution of the mixture fraction field*

The last part of this work is a study of the parallel evolution of both the spray segregation and the mixture fraction field during the evaporation process. As detailed above, among the various ways to describe this field we selected a spectral formulation that may be used for both dispersed and gaseous phases.

Stationary spectra of the liquid density fluctuations ξ' are plotted in figure 17 for the three standard Stokes numbers $St = 0.17$, $St = 1.05$ and $St = 5.6$, along with that of the turbulent velocity field. A discussion of the energy levels of these spectra
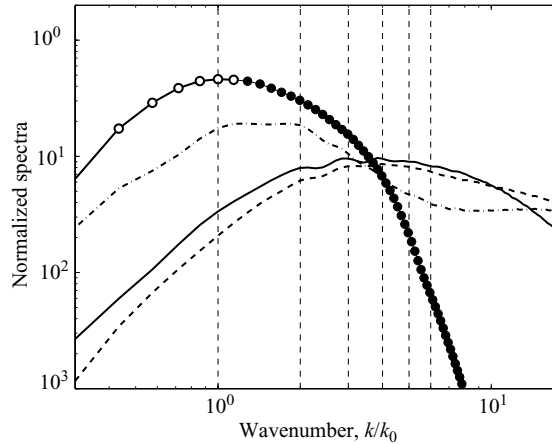
FIGURE 17. Variance normalized stationary spectra of ξ fluctuations when non-evaporating spray is in equilibrium. Symbols: carrier-phase kinetic energy spectrum (open circles: forced range, filled symbols: freely evolving range); dashed line: $St = 0.17$; solid line: $St = 1.05$; dot-dashed line: $St = 5.6$.

and their evolution is given conducted above through the analysis of the standard deviation of ξ and Z, and the corresponding spectra have been plotted in figure 9. Thus, to focus on the spectral and physical topologies of both fields, E_ξ and E_Z have been normalized by the variance of the field so that the integral of all the spectra presented is unity. Moreover, the wavenumber direction κ is normalized by k_0, the reference wavenumber of the turbulent velocity field corresponding to the frequency of the most energetic structures.

Before evaporation starts, the normalized shapes of the E_ξ spectra (figure 17) corresponding to configurations $St = 0.17$ and $St = 1.05$ are very similar, with a peak of energy centred in a frequency range three to four times greater than that of the turbulence. When $St = 5.6$, the low-frequency spectrum shape is different from the other two and very close to the shape of the velocity energy. The heavy droplets are mainly influenced by the large turbulent structures of the flow. On the other hand, the three spectra have high energy rates for the high frequency corresponding to the sampling of isolated droplets or small clouds of droplets.

The time evolution of normalized spectra E_Z (left) and E_ξ (right) is plotted for two different evaporation delays: $\tau_v = \tau_0/2$ in figure 18 and $\tau_v = 2\tau_0$ in figure 19 for three different Stokes numbers $St = 0.17$, $St = 1.05$ and $St = 5.6$ (from top to bottom). In each figure, several spectra are drawn: curves with square symbols represent the initial spectra corresponding to the beginning of the evaporation. Then the spectra (thin black curves) evolve towards the spectrum with circle symbols corresponding to the characteristic evaporation delay. Spectra evolving from this time are represented with grey lines.

Several general conclusions may be drawn from these figures. First, the time evolutions of all E_Z spectra clearly follow an identical path whatever the droplet's Stokes number and evaporation delay. When evaporation starts, the initial normalized mixture fraction spectra E_Z have exactly the same shape as the corresponding E_ξ spectra. However, diffusion and turbulent micro-mixing affect the evolution of E_Z whereas the modification of the droplet dynamics and evaporation changes E_ξ. Small structures in the mixture fraction due to isolated droplets or small clusters disappear
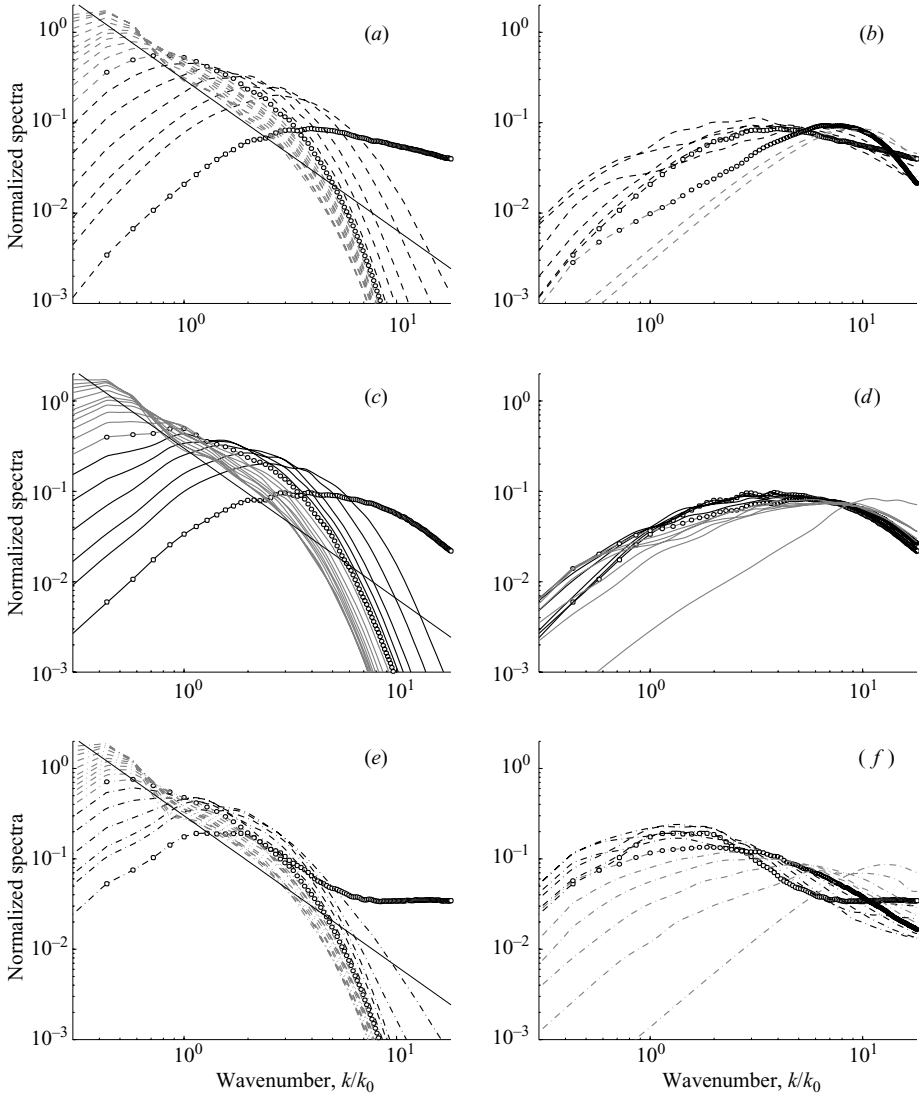
FIGURE 18. Time evolution of E_Z (left) and E_ξ (right) normalized spectra, $\tau_v = 0.5\tau_0$. Straight line: $k^{-5/3}$ range. Bold lines: evaporation starts, less-bold lines: time $< \tau_v$, symbols: time $= \tau_v$, grey lines: time $\geqslant \tau_v$. (a, b) $St = 0.17$, (c, d) $St = 1.05$, (e, f) $St = 5.6$.

very quickly and there is a shift of the peak of energy towards the low-frequency range. In other words, the characteristic size of the vapour pockets becomes progressively larger. This is a natural behaviour due to the disappearance of inhomogeneities because of turbulent mixing of the gas phase. Another contribution may be the stochastic behaviour of the droplets or small clusters leading to a vapour wake larger than the effective cluster size. During this process an inertial range appears on the mixture fraction spectra (figures 18 and 19, left). In a logarithmic representation, this range seems to converge towards the $k^{-5/3}$ limit that is shown on the figures. Particle density spectra are not affected by the appearance of an inertial range; this is a characteristic behaviour of turbulent gaseous mixing. As it has been described by Mydlarski & Warhaft (1998), this inertial range may be observed for all Reynolds
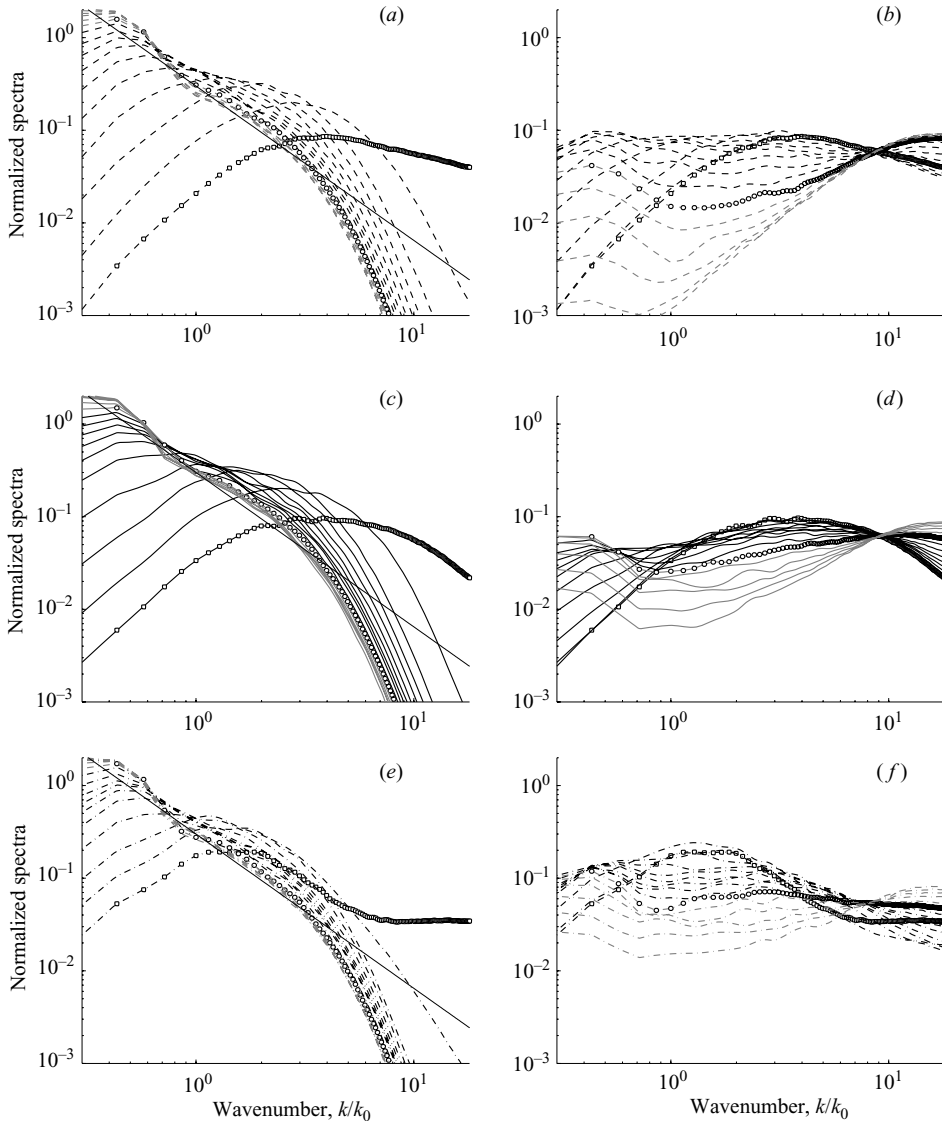
FIGURE 19. As figure 18 but for $\tau_v = 2\tau_0$.

numbers unlike the velocity spectrum that needs high values of Re. From this point of view, the spray evaporation has a weak effect on the shape of the scalar spectra. It appears that the time required to develop an inertial range does not depend on the evaporation delay. In fact, the effects of turbulence on the shapes of the E_Z spectra are more prevalent than the impact of the evaporation of the remaining droplets. Thus, in the configurations considered, the evaporation source terms mainly affect the energy level of the spectrum but not its shape, except in the early stages of the evaporation process where there exists a Stokes dependence of the length scale (similar when $St = 0.17$ and $St = 1.05$ and twice as large when $St = 5.6$). In that short period of time, the mixture fraction spectrum matches that of the clusters of droplets. This is confirmed by figures 20(a) and 21(a) where the characteristic length scales l_Z of the mixture fraction follow almost the same evolution whatever the
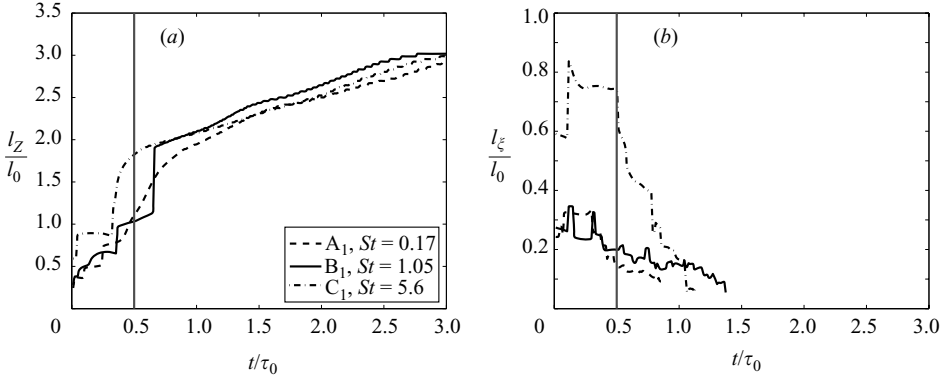
FIGURE 20. Time evolution of the length scales l_Z (a) and l_ξ (b), when $\tau_v = 0.5\tau_0$, corresponding to the size of the most energetic structures of the turbulent fields Z and ξ, respectively.
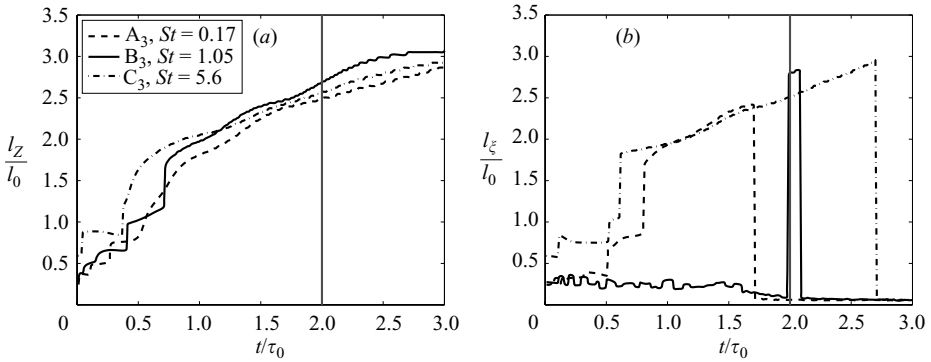

FIGURE 21. As figure 20 but when $\tau_v = 2\tau_0$.

evaporation delays or the Stokes number. Combustion is thus susceptible to being affected directly by the size of the clusters only if the ignition delays are short; otherwise, the main driving mechanisms will be the turbulent micro-mixing and the mean evaporation rate. Of course, it must not be forgotten that clusters of droplets may affect combustion processes in other ways, in particular through the momentum (drag forces) or temperature (droplet evaporation) coupling.

The evolution of the E_ξ spectra depends strongly on the droplet's Stokes number and the evaporation delay. As seen in figures 18 and 19, various behaviours may be considered. If $\tau_v = \tau_0/2$ and $t < \tau_v$ (figure 18), the spectrum shapes remain almost stationary. Then, in a second phase, there is a shift of the maximum of the spectra towards the high-frequency modes, implying a decrease of the characteristic size of the cluster of droplets because of the evaporation. This shift is more or less pronounced depending on the initial Stokes number of the droplet. This behaviour is shown graphically in figure 20(b) where l_Z is plotted for $St = 0.17$, $St = 1.05$ and $St = 5.6$ for $\tau_v = \tau_0/2$. The cluster size remains almost the same during the main evaporation process. But as soon as droplets begin to disappear, cluster sizes decay naturally. Note the quick evolution of the $St = 5.6$ case.

The E_ξ spectra of case $\tau_v = 2\tau_0$ (figure 19) have a very different evolution. Indeed, instead of keeping the same global shape and shifting towards high frequencies, a
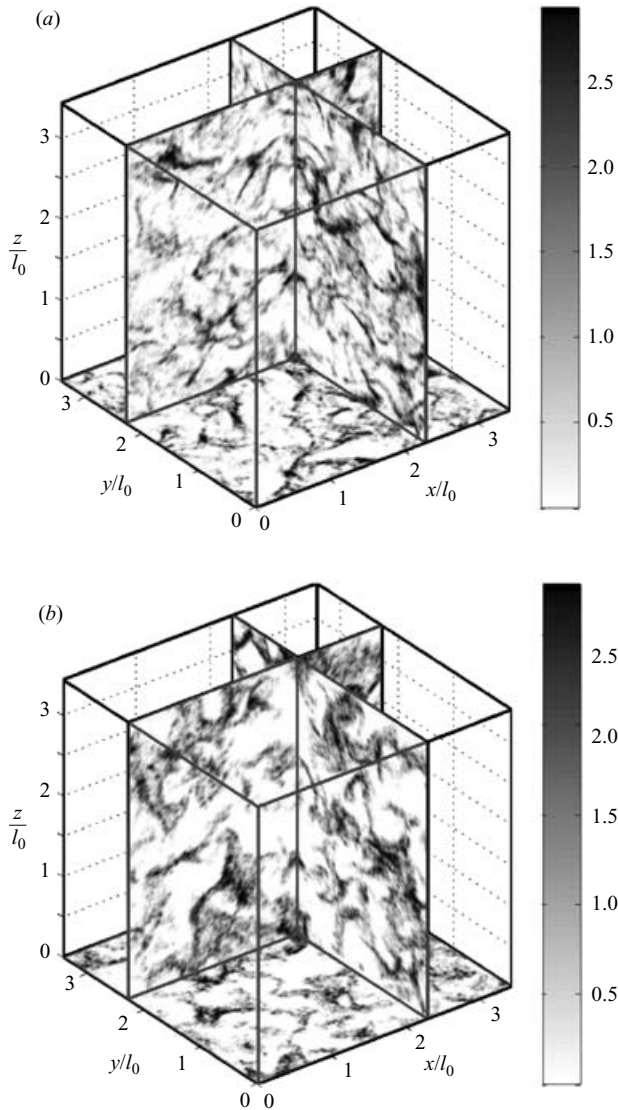
FIGURE 22. Spray density field when $t = \tau_v$ and $St = 5.6$. The remaining droplets are embedded in vapour pockets. (a) $\tau_v = 2\tau_0$, (b) $\tau_v = \tau_0/2$.

bimodal shape appears during evaporation. While the high-frequency range always sustains a high energy level, the energy of the intermediate-frequency range begins to decay strongly while the low-frequency energy increases. As soon as the characteristic evaporation delay is reached, low-frequency energy decays and the few remaining droplets concentrate the density fluctuations in the high-frequency modes, as might be expected. Considering these spectrum shapes, it appears that, for a while, two extreme characteristic length scales may be defined. This leads to a sudden modification of l_ξ (figure 21b) because each spectrum peak swaps from high frequency to low frequency. The specific appearance of a double length scale is confirmed in figure 22(a) where thin-fingered structures (small length scale) are emerging from clusters of droplets (large length scale). On the other hand, in figure 22(b) only one prevalent structure may be detected as confirmed by figure 18.

	$\overline{Z}$	Z'	$P(Z)$	E_Z	E_ξ
$(t \approx 0)$	$-$	$-$	$-$	$+$	$+$
$(0 < t \leqslant \tau_v)$	$+$	$+$	$+$	$+ \rightarrow - \ (1)$	$-$
$(\tau_v < t)$	$-$	$+$	$- \ (2)$	$-$	$+$

TABLE 2. List of the effects due to preferential segregation during the evaporation process. t is the simulation time to be compared with the evaporation delay τ_v. $+$ denotes a major effect while $-$ denotes a minor impact. (1) turbulence effects, (2) classical Gaussian shape.

5. Conclusion

Statistically stationary turbulence is used as carrier phase to study spray dispersion and evaporation using a spectral DNS solver where a semi-deterministic forcing scheme has been implemented. The evolution of the dispersed liquid phase is modelled using a classical Lagrangian description. A one-way coupling is applied between the Eulerian and Lagrangian solvers, except for the description of the vapour mass fraction evolution, which uses a two-way coupling. Consequently, turbulent flow characteristics remain constant while the dispersion of various sprays is studied. The sole effect of the droplet dynamics has thus been isolated and characterized for various sprays by prescribing Stokes numbers ranging between 0.025 and 11. The liquid density ξ is introduced to characterize droplet segregation properties. This quantity gives results similar to classical Lagrangian methods (Fessler *et al.* 1994) but deeper analysis is possible, in spectral space for example.

First, the dispersion of non-evaporating droplets is considered. It shows the formation of clusters of particles whose size and dynamics are strongly dependent on the Stokes number. This segregation effect is the result of three competing phenomena: the natural ejection of the droplets from the high-vorticity areas, the turbulent micro-mixing that affects the smallest droplets, and the ballistic effects, associated to the heaviest ones. In the second stage, droplet evaporation considered. This consequences of preferential segregation on the whole evaporation process are studied in detail from both the gaseous and liquid points of view. Several conclusions have been drawn from this study and are summarized in table 2.

Overall, the presence of droplet clusters due to preferential segregation is important for global variables such as the mean vapour mass fraction $\overline{Z}$ and its standard deviation Z', which are the key parameters of any combustion model. Hence the presence and properties of clusters must be accounted for. However, it appears that knowing the mean liquid density and its standard deviation is not sufficient to characterize the spray dispersion. An additional parameter, directly linked to droplet dynamics, such as the Stokes number, is thus necessary. Independently of the initial Stokes number, three stages can be defined for droplet evaporation:

(*a*) Single-droplet evaporation mode: far from saturation, there is no influence of clusters and an almost d-square law whose rate depends on isolated droplet characteristics is observed.

(*b*) Cluster evaporation mode: droplets are embedded in vapour pocket close to saturation. The evaporation rate strongly diminishes. It depends on the ability of the droplets to leave the saturated cloud (ballistic effect, high Stokes number) and on the gaseous diffusion flux from vapour saturated pockets towards low vapour concentration areas.

(*c*) Gaseous mode: the droplets have vanished or their number is no longer large enough to influence the gas-phase evolution. The classical turbulent mixing controls the vapour evolution.

During droplet evaporation, the mixture fraction field was also scrutinized. First, an analysis of the evolution of the PDF of the mixture fraction was carried out for three reference Stokes numbers. For very short times, the PDF shapes are not significantly different, and this corresponds to the single-droplet evaporation mode. However, as soon as vapour pockets reach the saturation level, PDFs are strongly affected. If ignition should occur at this moment, very different flames would be observed according to the droplet dynamics. Then, when the evaporation rates become negligible (gaseous mode) turbulent micro-mixing prevails and the mixture fraction PDFs relax towards a classical Gaussian shape. Finally, a joint spectral analysis of both the mixture fraction and liquid density spectra showed the strong impact of the cluster formation on the mixture fraction field, especially in the early stages of the evaporation process. However, turbulent mixing and gaseous diffusion prevail very quickly and vapour spectra relax towards a similar shape independently of their initial Stokes number. Note that the global energy level remains strongly affected by the liquid density spatial distribution. On the other hand, the liquid density spectra are strongly influenced by the droplet dynamics and differences still persist up to the end of the evaporation process. However, because the evaporation rate becomes negligible, the liquid density distribution no longer affects the mixture fraction field.

REFERENCES

ALISEDA, A., CARTELLIER, A., HAINAUX, F. & LASHERAS, J. C. 2002 Effect of preferential concentration on the settling velocity of heavy particles in homogeneous isotropic turbulence. *J. Fluid Mech.* **468**, 77–105.

BORGHI, R. 1988 Turbulent combustion modelling. *Prog. Energy Combust. Sci.* **14**, 245–292.

COLIN, O. & BENKENIDA, A. 2003 A new scalar fluctuation model to predict mixing in evaporating two-phase flows. *Combust. Flame* **134**, 207–227.

CROWE, C., SOMMERFELD, M. & TSUJI, Y. 1998 *Multiphase Flows with Droplets and Particles*. CRC Press.

DEMOULIN, F. X. & BORGHI, R. 2002 Modeling of turbulent spray combustion with application to diesel like experiment. *Combust. Flame* **129**, 281–293.

ELGOBASHI, S. & TRUESDELL, G. C. 1992 Direct numerical simulation of particle dispersion in a decaying isotropic turbulence. *J. Fluid Mech.* **242**, 655–700.

ESWARAN, V. & POPE, S. B. 1988 Direct numerical simulations of the turbulent mixing of the passive scalar. *Phys. Fluids* **31**, 506–520.

FESSLER, J. R., KULICK, J. D. & EATON, J. K. 1994 Preferential concentration of heavy particles in turbulent channel flow. *Phys. Fluids* **6**, 3742–3749.

GIVI, P. 1989 Model free simulations of turbulent reactive flows. *Prog. Energy Combust. Sci.* **15**, 1–107.

GUICHARD, L., REVEILLON, J. & HAUGUEL, R. 2004 Direct numerical simulation of statistically stationary one- and two-phase turbulent combustion: a turbulent injection procedure. *Flow, Turbulence Combust.* **73**, 133–167.

KERR, R. M. 1981 Theoritical investigation of passive scalar such as temperature in isotropic turbulence. PhD thesis, Cornell University.

KLIMENKO, A. Y. & BILGER, R. W. 1999 Conditional moment closure for turbulent combustion. *Prog. Energy Combust. Sci.* **25**, 595–687.

KUO, K. K. 1986 *Principles of Combustion*. John Wiley and Sons.

LEE, S., LELE, K. & MOIN, P. 1991 Numerical simulations of spatially evolving compressible turbulence. *Center for Turbulence Research, Annual Research Briefs, Stanford*, 126.

LELE, S. K. 1992 Compact finite difference schemes with spectral like resolution. *J. Comput. Phys.* **103**, 16–42.

LINÁN, A. & WILLIAMS, F. 1993 *Fundamentals Aspects of Combustion*. Oxford University Press.

LING, W., CHUNG, J. N., TROUTT, T. R. & CROWE, C. T 1998 Direct numerical simulation of a three-dimensional temporal mixing layer with particle dispersion. *J. Fluid. Mech.* **358**, 61–85.

MANTEL, T. & BORGHI, R. 1994 A new model of premixed wrinkled flame propagation based on a scalar dissipation equation. *Combust. and Flame* **96**, 443–457.

MASHAYEK, F. 1998 Direct numerical simulations of evaporating droplet dispersion in forced low Mach number turbulence. *Intl J. Heat Mass Transfer* **41** (17), 2601–2617.

MASHAYEK, F., JABERI, F. A., MILLER, R. S. & GIVI, P. 1997 Dispersion and polydispersity of droplets in stationary isotropic turbulence. *Intl J. Multiphase Flow* **23** (2), 337–355.

MILLER, R. S. & BELLAN, J. 1999 Direct numerical simulation of a confined three-dimensional gas mixing layer with one evaporating hydrocarbon-droplet-laden stream. *J. Fluid Mech.* **384**, 293–338.

MILLER, R. S. & BELLAN, J. 2000 Direct numerical simulation and subgrid analysis of a transitional droplet laden mixing layer. *Phys. Fluid* **12**, 650–671.

MYDLARSKI, L. & WARHAFT, Z. 1998 Passive scalar statistics in high-pclet-number grid turbulence. *J. Fluid Mech.* **358**, 135–175.

NEWMAN, G. R, LAUNDER, B. E. & LUMLEY, J. L. 1982 Modeling the behaviour of homogeneous scalar turbulence. *J. Fluid Mech.* **111**, 217–232.

ORSZAG, S. A. & PATTERSON, G. S. 1972 Numerical simulation of three-dimensional homogeneous isotropic turbulence. *Phys. Rev. Lett.* **28** (2), 76–79.

OVERHOLT, M. R. & POPE, S. B. 1998 A deterministic forcing scheme for direct numerical simulation of turbulence. *Computers Fluids* **27**, 11–28.

PANTANO, C., SARKAR, S. & WILLIAMS, F. A. 2003 Mixing of a conserved scalar in a turbulent reacting shear layer. *J. Fluid Mech* **481**, 291–328.

PETERS, N. 1986 Laminar flamelet concepts in turbulent combustion. In *Proc. 21st Symposium (Intl) on Combustion*, pp. 1231–1250. The Combustion Institute.

POINSOT, T., CANDEL, S. & TROUVÉ, A. 1996 Direct numerical simulation of premixed turbulent combustion. *Prog. Energy Combust. Sci.* **12**, 531–576.

POINSOT, T. & VEYNANTE, D. 2001 *Theoretical and Numerical Combustion*. Edwards.

REVEILLON, J., BRAY, K. N. C. & VERVISCH, L. 1998 DNS study of spray vaporization and turbulent micro-mixing. *AIAA Paper* 98-1028.

REVEILLON, J. & VERVISCH, L. 2000 Accounting for spray vaporization in non-premixed turbulent combustion modeling: A single droplet model (SDM). *Combust. Flame* **1**, 75–90.

REVEILLON, J. & VERVISCH, L. 2005 Analysis of weakly turbulent diluted-spray flames and spray combustion regimes. *J. Fluid Mech.*, **537**, 317–347.

RILEY, J. J. & PATTERSON, G. S., JR 1974 Diffusion experiments with numerically integrated isotropic turbulence. *Phys. Fluids* **17**, 292–297.

ROGALLO, R. S. 1981 Numerical experiments in homogeneous turbulence. *NASA, Tech. Mem.* 81315.

SAMIMY, M. & LELE, S. K. 1991 Motion of particles with inertia in a compressible free shear layer. *Phys. Fluids* **8**, 1915–1923.

SIGGIA, E. D. & PATTERSON, G. S. 1978 Intermittency effects in a numerical simulation of stationary three-dimensional turbulence. *J. Fluid Mech.* **86**, 567–592.

SIMONIN, O., FEVRIER, P. & LAVIÉVILLE, J. 1993 On the spatial distribution of heavy-particle velocities in turbulent flow: from continuous field to particulate chaos. *J. Turbulence* **118**, 97–118.

SIROVICH, L. 1991 *New perspectives in Turbulence*. Springer.

SQUIRES, K. D. & EATON, J. K. 1991 Preferential concentration of particles by turbulence. *Phys. Fluids* **3**, 1169–1178.

VERVISCH, L. & POINSOT, T. 1998 Direct numerical simulation of non-premixed turbulent flame. *Annu. Rev. Fluid Mech.* **30**, 655–692.

WANG, L. P. & MAXEY, M. R. 1993 Settling velocity and concentration distribution of heavy particles in homogeneous isotropic turbulence. *J. Fluid Mech.* **256**, 27–68.